Late Quaternary sea-level change and evolution of Belfast Lough, Northern Ireland: new offshore evidence and implications for sea-level reconstruction.

(Running title: Late Quaternary sea-level change and evolution of Belfast Lough)

Ruth M.K. Plets[*1]

S. Louise Callard[2]

J. Andrew G. Cooper[1]

Joseph T. Kelley[3]

Daniel F. Belknap[3]

Robin J. Edwards[4]

Antony J. Long[2]

Rory J. Quinn[1]

Derek W.T. Jackson[1]

[*] Corresponding author: Ruth Plets, School of Geography and Environmental Sciences, Ulster University, Coleraine, BT52 1SA, Northern Ireland; email: r.plets@ulster.ac.uk

[1] School of Geography and Environmental Sciences, Ulster University, Coleraine, BT52 1SA, Northern Ireland

[2] Department of Geography, Durham University, South Road, Durham,DH1 3LE, UK

[3] School of Earth and Climate Sciences, 5790 Bryand Global Sciences Center, Orono, ME 04469, USA

[4] Department of Geography, Museum Building, Trinity College Dublin, Dublin 2, Ireland

Late Quaternary sea-level change and evolution of Belfast Lough, Northern Ireland: new offshore evidence and implications for sea-level reconstruction.

Ruth M.K. Plets, S. Louise Callard, J. Andrew G. Cooper, Joseph T. Kelley, Daniel F. Belknap, Robin J. Edwards, Antony J. Long, Rory J. Quinn, Derek W.T. Jackson

Abstract

The interplay of eustatic and isostatic factors causes complex relative sea-level (RSL) histories, particularly in paraglacial settings. In this context the past record of RSL is important in understanding ice-sheet history, earth rheology and resulting glacio-isostatic adjustment. Field data to develop sea-level reconstructions are often limited to shallow depths and uncertainty exists as to the veracity of modelled sea-level curves.

We use seismic stratigraphy, 39 vibrocores and 26 radiocarbon dates to investigate the deglacial history of Belfast Lough (Northern Ireland) and reconstruct past RSL. A typical sequence of till, glacimarine and Holocene sediments, is preserved. Two sea-level lowstands (both max. -40 m) are recorded at c. 13.5k and 11.5k cal a BP. Each is followed by a rapid transgression and subsequent periods of RSL stability. The first transgression coincides temporally with a late stage of Meltwater Pulse 1a and the RSL stability occurred between c. 13.0k and c. 12.2k cal a BP (Younger Dryas). The second still/slowstand occurred between c. 10.3k and c. 11.5k cal a BP.

Our data provide constraints on the direction and timing of RSL change during deglaciation. Application of the Depth of Closure concept adds an error term to sea-level reconstructions based on seismic stratigraphic reconstructions.

Keywords: post-glacial relative sea-level change, , high-resolution seismics, glacio-isostatic adjustment (GIA), stillstand/slowstand, Younger Dryas,

1. Introduction

Modelled curves depicting sea-level changes since the Last Glacial Maximum (LGM), differ greatly around the world, as a result of glacio-isostatic adjustment (GIA), subsidence and tectonic activity (Bassett *et al*., 2005; Lambeck *et al.*, 2014). With a few notable exceptions, observational records of former relative sea level (RSL) rarely extend beyond the late Holocene (before 8k a BP) and those that exist, have a greatly reduced temporal resolution.

In the Irish Sea, global and local influences interacted to produce one of the most complex deglacial sea-level histories on earth. For many decades, field data from around the Irish Coast have been studied to understand the impact of isostasy on RSL changes (e.g. Carter *et al.*, 1989; Devoy, 1983; Devoy, 1991). Meanwhile, ice-sheet history in Great Britain and Ireland is actively being investigated (Clark *et al*., 2018) and despite recent advances (e.g. Chiverrell *et al*., 2013), uncertainties about the spatial extent and temporal thickness of ice hamper development of numerical models of RSL change. Consequently, GIA based reconstructions not only show high variability across the region (Brooks *et al*., 2008; Bradley *et al.,* 2011; Kuchar *et al.,* 2012), but there are also substantial differences between predicted RSL changes produced by different GIA models. Misfits between GIA model outputs and field data also create polarised views on the accuracy of such models (McCabe, 2008; Edwards *et al*., 2008) and the paucity of observational data before ca. 8k a BP from the Island of Ireland (Edwards and Craven, 2017) hinders further progress.

Here, new observational data based on multibeam bathymetry, 260 km of seismic reflection records, 39 vibrocores and 24 radiocarbon dates are used to develop a new reconstruction of RSL history for Belfast Lough, on the east coast of Northern Ireland (Figure 1). As well as new data, previously collected offshore data from the same study area (Kelley *et al.*, 2006) have been incorporated into the analysis. Belfast Lough occupies a significant location in the Irish Sea and its RSL history is key to understanding regional and local ice-sheet history and GIA.

2. Geological and oceanographic setting

Belfast Lough is a meso-tidal marine embayment in the NW Irish Sea (Figure 1). The Lough and valley of the River Lagan, which drains into it, forms a broad trough underlain by soft Triassic marls and sandstones (Lamplugh *et al*., 1904). The region is mostly covered by widespread deposits of glacial origin which consist mainly of glacial diamict, with extensive spreads of sand interbedded or superimposed (Manning *et al*., 1970). Apart from being ice-covered during the LGM, the region underwent two subsequent readvances: (1) the Killard Point Readvance of Irish Ice (17.3-16.6k cal a BP (McCabe and Clark, 1998; Ballantyne and Ó Cofaigh, 2017)) and (2) the East Antrim Coastal Readvance of Scottish Ice (occurring either at c. 16.5k cal a BP (Finlayson *et al.,* 2014) or c. 15.6–15.0k cal a BP (McCabe and Williams, 2012)). The latter shaped much of the drumlinised landscape. The city of Belfast is largely built on Holocene estuarine clays, which locally overlie freshwater peats that extend to -12 m (OD Belfast) (Manning *et al*., 1970).

The river Lagan enters the head of the Lough. Some authors (Lamplugh *et al.,* 1904; Manning *et al*., 1970) suggest ice-ponding during retreat of Scottish ice may have blocked the river, creating a "Glacial Lake Lagan", with associated glacio-lacustrine sedimentation. None of these sediments, however, have been dated.

A deglacial RSL reconstruction for NE Ireland, solely based on field observations along a stretch of 200 km of coastline and spanning 20 to 12k a BP (McCabe *et al*., 2007; Pink line Figure 2), suggests that, regionally, sea level was initially high due to isostatic depression. This is followed by a -30 m lowstand around 13.5k a BP, as derived from dated vibrocore samples collected in Belfast Lough by Kelley *et al*. (2006). Overall, this reconstruction suggests very rapid and large RSL changes. In contrast, more local RSL curves for the North Down area (centred around Belfast Lough) derived from GIA models (Brooks *et al*., 2008 (Model E); Bradley *et al.,* 2011; Kuchar *et al.,* 2012), show a monotonic drop in RSL from an early deglacial highstand (Figure 2). The three GIA model-derived reconstructions show successive RSL lowstands at ~14.5k and ~11k cal a BP, separated by a higher RSL inflection at ~13.5k cal a BP and followed by a Holocene highstand ~7k cal a BP. However, RSL predictions differs by up to 20 m between models, caused by differences in the choice of the regional ice-sheet reconstruction for the British-Irish ice sheet. The scarcity of data and lack of sea-level index points before 12k cal a BP hamper efforts to resolve these differences.

3. Methods

Seismic Pinger data and 39 vibrocores were acquired and analysed. Multibeam data were made available to the project. The methodology is similar to that discussed in Plets *et al*. (2015). Full details are provided in the supplementary section. All data are reduced to lowest astronomical tide (LAT), which is 2 m below Ordnance Datum Belfast, 1958 (OD).

4. Results

4.1. Seabed morphology

Belfast Lough is a 40 km-long funnel-shaped embayment, 20 km wide at its mouth (Figure 1). It shallows rapidly landward from about 190 m to 10 m. Bedrock outcrops are common on the margins, but sediment occurs through most of the Lough.

The mouth of the Lough contains three areas of complex seafloor morphology. Just northwest of the Copeland Islands are several flat-topped shoals in depths of 15 m - 20 m (Figure 1b, zone 1). Below 20 m depth, the shoal tops are rounded. Near the planed-off shoals, in a depth of about 30 m, a c. 500 m wide, c. 5 m high, arcuate ridge extends for 5 km towards the north (Figure1b, zone 2). On the NW margin of the mouth of the Lough, the seafloor has an irregular topography, with ENE-WSW oriented ridges (usually less than 1 m in relief) (Figure 1a, zone 3). Further east, in water depths between 120 – 150 m, the hummocky terrain has been reworked by tidal currents, giving it a 'smeared' appearance (Figure 1a, zone 4).

4.2. Seismic stratigraphy

Five units identified from seismo-stratigraphic analysis of the pinger data are described below (summarized in Table 1, Figure 3 and 4):

Unit 1 (U1) is the deepest unit imaged. Reflectors within the unit are of medium amplitude and frequency and display a chaotic configuration. The surface, S1, overlying this unit is mostly continuous and is characterized by an irregular topography.

Unit 2 (U2) overlies U1 in most areas. Reflectors within the unit are disrupted and mostly discontinuous, with relatively low amplitudes. The unit crops out on the northern side of the Lough as a hummocky terrain (Figure 1, zone 3). The lower reflectors onlap onto Surface S1, whilst the top reflectors are truncated by Surface S2. This latter surface is mostly discontinuous with an irregular topography. A grid of surface S2 shows that U2 forms a raised NNW-SSE ridge that divides the Lough into two sections: a western inner basin and eastern sloping surface (Figure 4a).

Unit 3 (U3) can be divided into two facies, onlapping onto Unit 2: Fs3a in the inner basin to the west of the U2 ridge, and Fs3b to the east. Reflectors in Fs3a are higher amplitude, mostly wavy and parallel. Fs3b consists of medium amplitude reflectors that appear contorted and chaotic. Whilst Fs3a is truncated by surface S3, this truncation becomes less defined on the top of Fs3b. Below 40 m LAT depth, S3 can usually no longer be detected. The thickness map (Figure 4b) shows that this unit infills depressions seen in S2 (Figure 4a; top of U2), with the main depositional centre (up to 20 m thick) to the east of the U2 ridge. To the east, the unit is <10 m thick. U3 is thin to absent on top of the ridge. S3 is a regular, smooth and flat surface in the Inner Lough with an average depth between -16 and -17 m (LAT). The surface becomes irregular over the ridge, after which it drops off to a depth of -40 m (Figure 4c).

Unit 4 (U4) appears as a thin ‘fuzzy’-looking unit above U3 and dominates the inner lough area. It forms a chaotic, high amplitude band bounded by the erosional surface S3 at the bottom and S4 at the top. The top surface appears disconformable but its continuity is disrupted throughout. The depositional centre of this unit is to the west of the ridge (Figure 4d) where it can reach up to 3 m. To the east of the ridge, U4 thins downslope. The thinning continues until S3 and S4 merge, before becoming indiscernible at depths around -40 m. S4 (Figure 4e) forms a flat, smooth surface in the Inner Lough with a depth around -15 m -16 m (LAT), sloping down beyond the buried U2 ridge system.

Unit 5 (U5) is divided into two facies: the bottom (Fs5a) is largely transparent; the top (Fs5b) has medium amplitude and frequency internal reflectors. The depositional centre of U5 is

seaward of the ridge, reaching thicknesses up to 10m (Figure 4f). In the Inner Lough, U5 is rarely >5m thick.

4.3 Litho-biostratigraphy and radiocarbon dates

Lithofacies description and dates

Logging and sampling of the 39 cores, reveal 8 lithofacies assemblages based on texture and sedimentary structures. These are described below from bottom to top (Figure 5, Figure S1; for detailed biostratigraphic detail see Table S1). Radiocarbon dates were obtained from shells and foraminifera in the cores to bracket the ages of distinct boundaries (Table 2; Figure 5b).

Lithofacies A comprises a laminated reddish brown very fine sand with a minimum thickness of 1 m (Figure S1c). This unit was only retrieved in two cores (BL44 and 45) located in water depths below 40 m. Foraminifera were present are low abundance, hence, no counts were performed and no dates were obtained.

Lithofacies B is a massive medium, well-sorted sand with few shell fragments. In deep water (>40 m), the sand is fine-grained with fine laminations. It is at least 1.5 m thick and does not occur in the Inner Lough. No foraminifera counts were performed due to the low abundance and no dates were obtained.

Lithofacies C is a stiff, reddish-brown clay, with fine sand laminations or lenses (lenticular bedding) and disseminated organic material (Figure 5a, Figure S1a and b). The laminations predominantly occur at the top and are often contorted and, in some instances, sheared with a vertical offset of a few centimetres. A few rounded pebbles are present within the clay matrix. A high organic content is indicated by rapid oxidation of black clays to brown when exposed to the air – the black colour is more prominent at the bottom. The upper surface is usually erosional with bioturbation evident. The unit was never fully penetrated but reached a thickness of at least 80 cm. Seven foraminifera samples were taken, in which the glacimarine species *Elphidium excavatum forma clavatum* was found as dominant. Dates from this species range between 13.0-12.2k cal a BP, consistent with deposition during the Younger Dryas (ca. 12.9-11.5k cal a; Rasmussen *et al*., 2006).

Lithofacies D is a mostly fine sand to silty-sand unit, characterised by large shells at the top (sometimes oysters) and smaller bivalves (mostly articulated) at the bottom. Occasional rounded pebbles (2-3 cm diameter) rest on the erosional surface (Figure 5a, Figure S1a and b). Rare rip-up clasts of the underlying Facies C are present. The unit is usually 30–40 cm thick. Seven foraminifera assemblage counts showed a mixed population with marine, estuarine/brackish and shallow glacimarine species all present in significant numbers (Table S1). *Elphidium excavatum forma clavatum* dominates in the inner Lough whilst the outer

Lough cores are dominated by the inner shelf species *Cibicides lobatulus*. Paired dating of foraminifera and bivalve shells was performed for two samples, with a further 6 dates from single whole shells (Table 2, Figure 5b). The dates for the foraminifera occur within the age range of the Younger Dryas (12.8-12.0k cal a BP), whilst the (paired) shells are much younger. In the inner Lough (BL9, 39), shell ages range between 11.5-10.3k cal a BP. Close to the U2 ridge (BL 17, 13), ages are c. 8.8k cal a BP at the top of the unit; in the deepest core sampled (BL29), the oldest age of 14,914±458 cal a BP was found for an unpaired bivalve while a younger shell sampled only 10 cm higher has an age of 12,340±235 cal a BP.

Lithofacies E is a massive silty to sandy-silt unit containing abundant small bivalve shells (*Corbula gibba*), the concentration of which decreases upwards. The boundary with the overlying lithofacies F is gradual, whilst the boundary with the underlying lithofacies D is sharper (Figure 5a). The inner Lough shows an equal mix of marine, inner-shelf, estuarine and glacimarine foraminifera species (*Elphidium excavatum*, *Elphidium excavatum forma clavatum* and *Ammonia becarrii;* Table S1). The deeper cores contain fewer foraminifera, dominated by marine and inner-shelf species. Shells range in age between 7.8-9.0k cal a BP (Table 2, Figure 5b).

Lithofacies F is a fining-upwards silty clay containing abundant gastropod *Turritella* sp. shells (Figure 5a). It is typically 2 m thick and occurs throughout the inner lough. In the inner Lough, the top of this unit is dominated by marine/inner-shelf and inner-shelf/estuarine species (*Rosalinia anomala, Asterigerinata mamilla, Elphidium excavatum, Cibicides lobautuls*, *Quinqueloculina* sp. and *Elphdium gerthi;* Table S1). In deeper water, foraminifera concentrations are very low and dominated by marine/inner-shelf and inner-shelf/estuarine species (*Cibicides lobatulus* and *Asterigerinata mamilla;* Table S1). In the inner Lough, a *Turritella* shell date suggests transition into this unit around 7.4k cal a BP (BL16) with an earlier transition around 9.1k cal a BP in deeper water (BL13). A paired foraminifera date yielded a Younger Dryas age, suggesting continued reworking of foraminifera. Towards the top of the unit, shell ages range between 4.9–5.4k cal a BP (BL9, BL39) (Table 2, Figure 5b).

Lithofacies G comprises a massive, stiff brown/grey silt or clay with varying proportions of shell fragments. It is typically 30 cm thick and forms the modern seabed in only a few cores (BL12, 14, 17, 37) towards the inner reaches of the Lough. Foraminifera are present but were not analysed, and no dates were obtained.

Lithofacies H comprises a coarsening upwards grey silty medium to fine sand with shell fragments in varying abundance (Figure 5a). It forms the surface unit in most cores, is typically 0.5 m thick and often rests on an erosional surface. One foraminifera count shows the assemblage to be dominated by inner-shelf marine species (*Ammonia batavus* and *Cibicides lobatulus;* Table S1).

As well as the dates obtained for this project, there are a further four published dates (Kelley *et al*., 2006; Table 2). Two further dates were obtained from Kelley *et al.'s* (2006) core BL03-04 in 2008 (unpublished) from a disarticulated infaunal bivalve and a *Portlandia arctica* shell (Table 2). The latter provides the oldest date from Belfast Lough (15,668±293 cal a BP) and was obtained in the red stiff clay found at the bottom of BL03-04 (here labelled Lithofacies I; Figure S1). Shells from the unit above the red sediments date between 13.1-13.7k cal a BP. The Younger Dryas sediments which dominate the Inner Lough appear to be absent in the outer Lough. Kelley *et al*. (2006) also described a second core, taken 50 m to the SW of BL03-04. A date from a *Spisula sp.* shell recovered from the stiff red clay returned an age of 13.5k cal a BP. This is similar to dates found for the shells in the coarse sand layer above this unit, which is a more typical habitat for *Spisula sp.*, and suggests the shell burrowed into the lower unit.

Core stratigraphy

The stratigraphy varies with position in the Lough (Figure 5b, 6, S2). In the inner Lough (c. 7-11 m water depth), the base of the cores consists of black, laminated stiff clay (Lithofacies C). It grades upwards into red/brown laminated stiff clay with a few sand lenses towards the top, and occasional small pebbles. The unit is truncated by an erosional surface, above which sits a bioturbated silty to sandy unit with bivalves and occasional pebbles (Lithofacies D). The top of Lithofacies D is usually capped by sediment containing large shells. Above this is a silty clay with abundant small articulated bivalve shells (Lithofacies E). It grades upward into a silty clay unit, with abundant *Turritella sp.,* occasionally concentrated in shell lags (Lithofacies F). The top of the inner Lough cores consists of silty sand with abundant large shells and shell fragments (Lithofacies H). In a few locations in the innermost Lough, this is replaced by stiff grey mud or clay (Lithofacies G).

Most of the slope cores (12-30 m water depth) consist of silty or silty-sand material at the bottom. The deeper the location of the core, the coarser the basal unit. In one slope core (BL16), the lithologies are similar to those found in the inner Lough with stiff reddish-brown mud (Lithofacies C, at -19.9 m) at the base. In another (BL21), a red/brown clay rip-up clast from lithofacies C is included within the overlying silty facies, suggesting its extent to at least -24 m. Silty sand is succeeded by *Turritella*-rich silty clay (Facies F), with the modern seabed consisting of medium sand (facies H).

The Outer Lough cores (>30 m water depth) consist of a well-sorted, generally structureless medium sand (Lithofacies B). Occasional pebbles and shell layers are present. In the deepest cores, the sand is fine-grained and laminated. In two cores acquired in >40 m water depth, the sand is distinctly red and laminated (Lithofacies A; Figure S1c). In the outer Lough, core BL03-04 described by Kelley *et al*. (2006) consists of massive red clay with pebbles at the base (here annotated as Lithofacies I; Figure S1d). A dipping boundary marks the top of this unit, above which 20-30 cm of red laminated muds and sands occur. The colour of this unit is like that of lithofacies A, albeit with higher clay content. It is noted that both the massive clay and sandy laminations are distinctly different in colour than the

red/brown clay cored in the inner Lough. A pebbly coarse sand with abundant shells, similar to lithofacies D, sits on the laminated red sands and clays, with a clear boundary between them. A rip-up clast of red mud was found at the top of this unit.

5. Discussion

5.1. Overall stratigraphy

The combined data enable an interpretation of the nature and patterns of sedimentation and erosion in the embayment and provide insights into the associated RSL change. Starting with the oldest unit, the stratigraphy of offshore geology of Belfast Lough can be summarized as follows (for the interpretation of the seismic units, see Table 1):

Seismic unit U1 represents the acoustic basement and S1 is the irregular upper surface of the bedrock (Permo-Triassic sandstones).

Overlying the unconformity S1, U2 occurs mainly as a 15-20 m thick and 2.5 km wide NNW-SSE orientated ridge spanning across the Lough. U2 crops out on the NW margin of the Lough (Figure 1a, zone 3) and, with its irregular topography, is distinctly different from the surrounding seabed. It was not reached by cores but based on the seismic characteristics and appearance on the seabed, is consistent with till (Barnhardt *et al*., 1997). Based on its geomorphology and setting, the U2 ridge (Figure 4a) is tentatively interpreted as a moraine. SW of this ridge, near the Copeland Islands (Figure 1b, zone 1), the flat-topped shoals in water depths of 15–20 m are an extension of U2 and are interpreted as drumlins, planed off by wave erosion (Oldale *et al*., 1994; Shaw *et al*., 2011); below 20 m depth, the drumlins retain a rounded appearance. The hummocky terrain in deeper water (Figure 1a, zone 4) also resembles a drumlin field aligned along a NW-SE axis.

U3 drapes the underlying bedrock and till, and is focused in two depocentres (Figure 4b) divided by the till ridge. It is more extensive and thicker in the inner (western) basin (Fs3a) and is mostly absent on top of the ridge. The laminated nature of the sediments, and lack of basal erosion, suggests suspension settling and is consistent with deposition in a glacilacustrine or glacimarine setting (Barnhardt *et al*., 1997). As none of the inner Lough cores reached this unit, it cannot be determined whether these sediments were deposited in a marine environment and/or an ice-ponded lake (Lamplugh *et al*., 1904; Manning *et al*.,1970) – the latter remaining a plausible hypothesis. Kelley *et al*. (2006) succeeded in penetrating the upper part of unit Fs3b in the outer Lough (Lithofacies I; Figure S1). A *Portlandia arctica* shell, obtained from massive red clay with occasional pebbles (interpreted as dropstones), was dated to 15,6685±293 cal a BP (Table 2). The sediments display all the characteristics of a glacimarine origin, with the arctic shell species suggesting a cold environment. Whilst there is disagreement about when Scottish ice left the area after the East Antrim Readvance (McCabe and Williams, 2012; Finlayson *et al.,* 2014), these sediments indicate cold conditions continued until at least c. 15.7k cal a BP.

S3, an erosional unconformity, truncates U3 (glacimarine) and the top of the U2 till ridge (Figure 3). It is interpreted as a wave ravinement surface produced during a marine transgression (Catuneanu, 2006; Bache *et al*., 2014). The longitudinal profile of the ravinement surface shows it to be steep in the outer and near-horizontal in the inner Lough (Figure 4c). This surface was cored by Kelley *et al*. (2006) in the outer Lough and proved to be a 30 cm-thick sandy shell hash. Three radiocarbon dates obtained for these sediments yielded ages of 13.1-13.7k cal a BP (Table 2). These provide a date for the onset of the formation of the wave ravinement associated with a transgression phase. In one of the cores collected in this study (BL29; Figure 5b), a ravinement surface was encountered around -40.7 m LAT and was overlain by approximately 40 cm of large shells in a sandy matrix, similar to those encountered by Kelley *et al*. (2006). A shell positioned within the shell hash, yielded a date of 12,340±235 cal a BP. On the seismic reflection profiles, the surface extends to c. -40 m LAT. We discuss our interpretation of the depth of the wave ravinement surface in section 5.2, but the depth of the traced unconformity suggests that the lowstand preceding transgression was no lower than ~-40 m. S3 becomes near-horizontal in the inner Lough at a depth of ca. -17 m, suggesting a prolonged period of sea-level stability after the initial transgression.

U4 rests upon the erosional surface of S3 and is commonly 1.5 m thick (maximum 3 m). Its 'fuzzy' seismic signature (Figure 3) is similar to that found in gas-charged sediments (Judd and Hovland, 1992). In no core was its base reached. U4 is represented by lithofacies C which, with its lenticular bedding, bioturbation and sand lenses, is suggestive of deposition in a low energy, shallow water tidal environment (Davis and Dalrymple, 2012). The contorted bedding and occasional brittle deformation (Figure S1b) may reflect cold climate processes that caused freezing of the sediment (Allard *et al*., 1998). The occasional pebbles may represent dropstones. All radiocarbon ages indicate that this unit was deposited during the Younger Dryas between 13-12.2k cal a BP under cold conditions (Table 2). This was potentially initiated earlier since the unit was not cored in its entirety, and potentially lasted for longer, as the top has been eroded. The current consensus is that the Irish Sea and low ground in Ireland were free of (glacier) ice by 15k cal BP (Ballantyne and Ó Cofaigh, 2017), and that ice was limited to mountain cirque glaciation during the Younger Dryas (Gray and Coxon, 1991; Barr *et al.*, 2017). However, sea loughs may have become seasonally frozen in winter with sea-ice incorporating material (sand and small pebbles) from the coastal zone and depositing it in the Lough (Lisitzin, 2002). U4/lithofacies C is mainly present in the inner Lough and does not occur much further offshore beyond the till ridge (Figure 4d). In the outer Lough transgressive sediments directly overly the glacimarine unit (Kelley *et al*., 2006).

The top of U4 is marked by a high amplitude reflector (S4), indicated in cores to be an erosional surface above lithofacies C (Figure 5a, Figure S1b). This is interpreted as a second wave-cut ravinement surface created during a second transgression. S4 can be traced on the seismic data to depths of -40 m (Figure 4e), suggesting a second lowstand that reached no lower than -40 m. The sediments of Lithofacies D are interpreted as shallow water estuarine sediments, subject to higher energy conditions than lithofacies C. Concentrations of large

shells in the unit likely represent lag deposits. Paired dating shows that the foraminifera were reworked from the underlying Younger Dryas sediments, while the shells are distinctly younger (Table 2). The foraminifera assemblage counts contain species from different environments (Figure 5b, Table S1), pointing towards a dynamic setting with substantial reworking.

Seismic unit Fs5a (bottom U5) appears to coincide with lithofacies D as well as lithofacies E, representing the transition into a fully estuarine sedimentary environment. Lithofacies E lacks the *Turritella sp.* shells which are abundant in the overlying unit, but instead has a large concentration of small bivalves (Figure 5). The lack of *Turritella sp.* could indicate a large supply of sediment at that time, which would be disadvantageous to stationary feeders. The foraminifera counts show an increase in estuarine species compared to the underlying Lithofacies D (Figure 5b, Table S1), but show little distinction between Lithofacies E and F. Dating of the shells in Lithofacies E (7.8-9.0k cal a BP) points towards a potential erosional event in the inner Lough, with the underlying Lithofacies D likely to be older than 10.3k cal a BP (Figure 5b, Table 2).

The contact with the thicker overlying unit Fs5b (top U5) is a gradational, fining upwards into fine silts, interpreted as shallow subtidal estuarine sediments (Lithofacies F). The abundant *Turritella* shells are characteristic of such environments (Poirier *et al*., 2009) and high concentrations potentially mark changes in environmental conditions (Baltzer *et al*., 2015) or storm events. The mix of silt and sand suggests deposition in a low energy environment with pervasive bioturbation. All of this records a period of transgression and increasing water depths, confirmed by the foraminifera which show an increase in deeper marine species towards the top (Table S1). The radiocarbon dates also confirm the gradual transition with no indication of a time hiatus (c. 9.1k cal a BP for deeper parts; 7.4k cal a BP for the inner Lough; Figure 5b)).

The thin surface Lithofacies H and G are barely discernible in the seismic records, but a strong reflector underneath the seabed could indicate the change into more sandy sediments (Figure 6). This is ascribed to an increase in wave reworking as sedimentation and/or sea-level fall brings the sediment surface within the zone of increased wave action. Lithofacies H forms the modern seabed and is characteristic of the estuarine setting of the modern Belfast Lough. Lithofacies G is distributed in the upper reaches of the modern Lough and represents a proximal subtidal mudflat environment exposed to low wave energy and more fluvial influences. Two dates from the top of the underlying unit indicate that this unit is younger than c. 5.2k cal a BP (Table 2).

5.2. Late Quaternary evolution and the record of sea-level change

The combined seismic-, litho- and bio- stratigraphy and associated chronology point to a temporal succession of events that record relative sea-level changes during the early period of deglaciation through to the mid-Holocene. The sequence of events is outlined as follows and represents a minimum RSL reconstruction (i.e. sea level must have been above this (light grey line Figure 7b&c)):

1. Deposition of till, forming a ridge across the Lough. This could have happened during the LGM retreat or later re-advance phase (most likely the Killard Point Readvance (17.30-16.6 ka BP (McCabe and Clark, 1998; Ballantyne and Ó Cofaigh, 2017).
2. Drumlinisation during a subsequent phase of west-east ice movement tentatively linked to the East Antrim readvance (c. 16.5 ka (Finlayson *et al.,* 2014) or c. 15.6 – 15.0 ka cal BP (McCabe and Williams, 2012)), evidenced by onshore and submerged offshore drumlins near the Copeland Islands (Figure 1b zone 1).
3. Flooding of the basin and deposition of glacilacustrine/marine sediments. This is linked to high sea-levels associated with the glacio-isostatically depressed land immediately after ice retreat. The marine *Portlandia arctica* shell dated to c. 15.7k cal a BP (point (30) Figure 7a) correlates with a high RSL at that time, recorded at Rough Island in Strangford Lough, some 20 km south of the study area, where marine muds drape drumlins (15.0k cal a BP at +2.72 m OD (+4.72 m LAT) (McCabe and Clark, 1998; Brooks and Edwards, 2006; point (o) Figure 7a).
4. Subsequent land uplift caused RSL fall with the maximum depth of the (wave-cut) erosional unconformity represented by deepest occurrence of S3 around -40 m LAT (dashed yellow line Figure 7a). As this surface is wave cut, we tentatively put the maximum depth of the lowstand 2 m above this at -38 m. Dating of the topmost unit of the underlying sediment and the base of the overlying coarse transgressive sediments (Kelley *et al*. 2006; point (28) on Figure 7a), place the timing of this lowstand before c. 13.5k cal a BP but after the Rough Island date (15.0k cal a BP) (indicated as 'Maximum lowstand I', Figure 7b).
5. The subsequent transgression formed the erosional wave ravinement surface (S3), truncating the till ridge and glacimarine sediments. Three marine shell dates from the transgressive unit from the outer part of the Lough (Kelley *et al*. 2006; points (25, 26, 27) Figure 7a) suggest RSL had reached c. -30 m between c. 13.1 and 13.6k cal a BP. Landward of the till ridge, the flat nature of the surface suggests a period of RSL stability after transgression, with the unconformity sitting at about -17 m (dashed light green line Figure 7a). This RSL still-stand is consistent with the planation of the offshore drumlins at water depths between -15 m and -20 m (Figure 1b zone 1). Owing to the wave cut nature of the surface, the height of RSL is tentatively put at c. -15 m LAT (Light grey line Figure 7b&c).
6. On surface S3, tidally influenced sediments of U4/Lithofacies C accumulated in the inner part of the Lough (points (8, 18, 19, 24, 23) Figure 7a). This unit records a period of RSL stability (indicated as 'Stillstand I' Figure 7b) and rapid sediment accumulation, during the colder Younger Dryas. Joining the suggested position of RSL, as shown by the transgressive sediments in the outer Lough (points (25, 26, 27) Figure 7a), and the oldest date for the tidal sediments (c. 12.8k cal a BP (point (19) Figure 7a), provides a tentative indication of the rate of RSL rise prior to this stillstand.

7. The overlying erosional surface (S4) extends to -35-40 m LAT (dashed yellow line Figure 7a) and indicates RSL fell to a depth somewhat above that (tentatively placed at -38 m). Based on the dates of Lithofacies C and the overlying Lithofacies D, this occurred after c. 12.5 ka cal BP and prior to c. 11.3 ka cal BP (indicated as 'Maximum lowstand II' Figure 7b). These dates and the position of the maximum lowstand give a first indication of the possible rates of regression and transgression.
8. Surface S4 was then cut into U4/Lithofacies C during ongoing transgression. Wave reworking incorporated clasts and foraminifera (points (1, 3, 15, 17) Figure 7a) from Lithofacies C into the overlying silty sands of Lithofacies D. A second period of RSL stability, tentatively put at -13 m LAT, is inferred by the extensive wave-cut erosional surface in the Lough at -15 m LAT marking the top of unit U4/Lithofacies C (dashed dark green line Figure 7a). Shell dates above the transgressive surface suggests that this planation occurred between c. 10.3 and 11.5k cal a BP (points (16, 21, 22) Figure 7a; indicated as 'Stillstand II' on Figure 7b). The youngest date coincides with development of a freshwater peat deposit throughout the Belfast Lough area, dated to c. 10.3k cal a BP at -11.5 m LAT (Manning *et al*., 1970; minimum limiting date point (e) Figure 7a), whilst the older date matches that of a freshwater peat (11.4k cal a BP) from -8.6 m LAT (Carter, 1982; minimum limiting date point (g) Figure 7a). Peat is not preserved in the energetic environments of the Lough but is ubiquitous in the inner Lough and under Belfast City (Manning *et al*., 1970).
9. Continued transgression after c. 10k cal a BP, led to deeper water and less wave-influenced environments first characterised by bivalve-rich sands and silts (Lithofacies E; points (6, 7, 9, 10, 14) Figure 7a), followed by the appearance of *Turritella sp.* (Lithofacies F, point 5). This continued to the ca. +2 m mid-Holocene RSL highstand at c. 6.5k cal a BP (Carter, 1982).
10. A fall to the present sea level caused a lowering of wave base post c. 5.1k cal a BP, resulting in the deposition of fine sand seabed sediments (Facies A and B) and the disappearance of abundant *Turritella sp.* (youngest dated *Turitella sp.*, points (13 and 20) Figure 7a).

Whilst our sedimentary data do not provide primary RSL change evidence, they do provide, together with the ravinement surfaces data, constraints on the trajectory and timing of RSL. The ravinement surfaces are interpreted to be wave cut and are indicative of the depth at which the waves interact with the seabed. As a first estimate, our minimum RSL reconstruction placed RSL 2 m above any wave cut feature (light grey line Figure 7b&c). However, wave-induced sediment transport and morphological change potentially extends to wave base or Depth of Closure (DoC), defined as the depth at which wave-induced sediment transport and morphological change cease to be significant (Nicholls *et al*., 1998). The DoC is a concept routinely used in coastal and navigation engineering projects where sediment mobility needs to be calculated in the planning stage (e.g. Brutsché *et al*., 2016).

This concept has not yet been explored in sea-level reconstruction studies but can add an error estimate to offshore ground-truth data. The present-day DoC for the region is c. 7 m below mean water (Loureiro, pers. com., based on Hallermeier (1981); dark grey line Figure 7b). Ortiz and Ashton (2016) argue that the conventional techniques for calculating DoC are only valid for short (decadal) time scales. Their Morphodynamic Depth of Closure (MDoC) is representative of the maximum depth of wave influence at 10^2-10^3 year timescales. In the study area this could be as much as 14 m (black line Figure 7b). Applying these vertical error margins to our RSL reconstruction shows how these add a large potential sea-level range to the reconstruction. The (M)DoC calculation assumes that the wave regime and tidal range have not changed throughout the examined period. Palaeo-tide modelling around the British Isles (Scourse *et al*., 2018) suggests that a meso-tidal regime has persisted in the area since c. 16 ka BP. Despite these caveats, and because there is a lack of primary limiting dates, the reconstruction presented using the DoC is an important step forward in constraining RSL.

In Figure 7c this RSL reconstruction is compared against regional GIA model reconstruction outputs (Brooks *et al.,* 2008; Bradley *et al.,* 2011; Kuchar *et al.,* 2012) and McCabe *et al.*'s (2007) reconstruction. The GIA models vary from each other in that their earth models, global and regional ice-sheet reconstructions differ. Comparison is therefore important in that it provides a yardstick against which modellers can test their outputs. Three main observations can be made:

1. All three GIA-model-derived predictions and our RSL reconstruction indicate two lowstands after the East Antrim Readvance. However, the timing and depths differ. The earliest lowstand, caused by glacio-isostatic rebound after ice unloading, is represented by the erosional (transgressive) surface cored by Kelley *et al*. (2006). This is dated to between c. 13.4 and 15.0 cal ka BP, based on material dated above this surface and the Rough Island date. The observations made in this study suggest that the transgression potentially started somewhat later than the time shown by GIA-model-derived predictions and earlier than McCabe *et al*.'s (2007) reconstruction, but we lack further dates to narrow this down. The latest possible occurrence is displayed on the reconstruction. The second erosional (transgressive) surface was only cored in the inner Lough, but its offshore extension is evident in the seismic data. Our dates suggest that the associated lowstand occurred after c. 12.5 but before c. 11.3k cal a BP, putting it potentially up to 1000 years earlier than the second lowstand of the GIA model outputs. The maximum DoC lowstand (dashed dark grey bars) places these lowstands significantly lower (c. 20 m) than the lowest modelled lowstand (Brooks *et al*., 2008). Even the MDoC puts the depth of the lowstand (black dashed bars) over 10 m lower than the Brooks *et al*. (2008) curve. In McCabe *et al.*'s (2007) reconstruction, the first lowstand is close to MDoC's maximum lowstand.

2. Two clear transgressive events follow the lowstands. These are preserved as coarse shell-rich material, including pebbles, overlying a distinct erosional boundary. The start of

the rapid RSL as seen in the models corresponds to the inclusion of a meltwater pulse (MWP-1A) in the eustatic component of the GIA models between 14.5 and 13.5k cal a BP (Figure 7c, purple bar). Our suggested later start of the transgression is slightly out of sync with the onset of this event. However, recent results (Yokoyama *et al*., 2018) suggest that MWP-1A happened as a series of steps with the last pulse coinciding closely with the latest possible onset of the first transgression (Figure S3).

The start of the second transgression appears to correspond temporally with the initiation of MWP-1B around c. 11.5k cal a BP (Liu and Milliman, 2004), an event which is heavily contested (Bard *et al.,* 2016) and is not included in the global GIA models. In Belfast Lough, the magnitude of this transgression is potentially of the same order as the first transgression. Whilst there is still discussion and uncertainty about the timing, magnitude and existence of MWP-1B, our field data suggest an increased rate of RSL rise between 12.5-11.3k cal a BP. This is in general agreement with an increased rate in RSL rise in the global eustatic curve at that time (Figure S3).

3. Our data indicate two RSL still/slowstands which do not appear in regional GIA-model-derived reconstructions. A Younger Dryas stillstand has also been recognised in the Western Pacific (Liu and Milliman, 2004) and the Barbados coral record (Abdul *et al*., 2016), although the latter is contested (Bard *et al*., 2016). Major shoreline complexes developed during this 'slowstand', have been recognised in the south Atlantic (Cooper *et al*., 2017) and Indian Ocean (Green *et al*., 2014). In Belfast Lough, the sediments (resembling glacimarine sediments with dropstones and brittle deformation), foraminifera (glacimarine species *Elphidium excavatum forma clavatum*), radiocarbon dates and seismic data confirm a cold climate coupled with a stable RSL during the Younger Dryas. Dates for the second slowstand were obtained from the transgressive unit sitting on a clear, mostly flat, erosional surface as seen on the seismics and cored in the inner Lough. After this final still/slowstand, minimum limiting dates are available for the area (Brooks *et al*., 2008) and suggest a RSL rise until the mid-Holocene maximum.

6. Conclusion

The data from this study record a typical glacial-deglacial sedimentary sequence of infilling of a marginal marine embayment. The presence of drumlins and a potential moraine at the entrance of Belfast can aid in the reconstruction of the glacial history, indicating a potential readvance or stillstand. Unfortunately, the glacimarine sediments were not cored in the inner part of the Lough. A distinct Younger Dryas deposit was imaged and cored, indicating cold conditions with potential seasonal sea-ice, as well as a RSL still/slowstand. It is the first time this has been encountered in a shallow marine environment in Ireland and it forms an important marker for future seismic and coring work.

From a sea level's perspective, this paper potentially presents the most complex published record of local RSL changes. The data show evidence for two wave cut erosional

surfaces, suggestive of two lowstands, followed by two transgressions and two slowstands. Currently, such surfaces are disregarded by RSL modellers, as they represent marine limiting dates only, which cannot constrain more precisely the position of RSL. To enhance the utility of these surfaces in RSL reconstruction, the concept of the Depth of Closure has been explored for the first time. Whilst the technique requires knowledge of the past wave and tidal regime, it is an important step towards addressing depth uncertainties associated with marine data. This concept has not been explored elsewhere for past RSL reconstructions and further validation of the technique could lead to significant progress.

7. Acknowledgements

This study is part of the NERC funded project NE/H024301/1, “Late Glacial Sea Level Minima.” Thanks to Fabio Sacchetti, INFOMAR, MI, GSI, Connor McCarron, Will Evans, Andy Green, Master and crew of RV Celtic Explorer and RV Celtic Voyager. We thank Dr Xiaomei Xu at the Keck C cycle AMS Lab, University of California, for analysing the small radiocarbon samples. IHS provided Kingdom Suite the University Gift Programme. The multibeam dataset contains public sector information, licensed under the Open Government Licence v3.0, from the Ministry of Defence and the UK Hydrographic Office. This work was supported by the NERC Radiocarbon Facility NRCF010001 (allocation number 1683.1112). Finally, thanks to two anonymous reviewers who provided detailed comments and suggestions to improve this manuscript.

References

Abdul NA, Mortlock RA, Wright JD, Fairbanks RG. 2016. Younger Dryas sea level and meltwater pulse 1B recorded in Barbados reef crest coral Acropora palmata. *Paleoceanography* **31**: 330-344.

Allard M, Michaud Y, Ruz M-H, Héquette A. 1998. Ice foot, freeze-thaw of sediments, and platform erosion in a subarctic microtidal environment, Manitounuk Strait, northern Quebec, Canada. *Canadian Journal of Earth Sciences* **35**: 965-979.

Bache F, Sutherland R, King PR. 2014. Use of ancient wave-ravinement surfaces to determine palaeogeography and vertical crustal movements around New Zealand. *New Zealand Journal of Geology and Geophysics* **57**: 459-467.

Bard E, Hamelin B, Deschamps P, Camoin G. 2016. Comment on "Younger Dryas sea level and meltwater pulse 1B recorded in Barbados reefal crest coral Acropora palmata" by N. A. Abdul et al. *Paleoceanography* **31:** 1603–1608.

Bassett SE, Milne GA, Mitrovica JX, Clark PU. 2005. Ice sheet and solid earth influences on far-field sea-level histories. *Science* **309**: 925-928.

Ballantyne CK, Ó Cofaigh C. 2017. The Last Irish Ice Sheet: Extent and Chronology. In *Advances in Irish Quaternary Studies,* Coxon P, McCarron S, Mitchell F (eds). Atlantis Press, Atlantis Advances in Quaternary Science 1: 101-150.

Baltzer A, Mokeddem Z, Goubert E, Lartaud F, Labourdette N, Fournier J, Bourillet, J. 2015. The "Turritella Layer": A Potential Proxy of a Drastic Holocene Environmental Change on the North–East Atlantic Coast. In *Sediment Fluxes in Coastal Areas*, Maanan M, Robin M (eds). Coastal Research Library, vol 10. Springer, Dordrecht.

Barr ID, Roberson S, Flood R, Dortch J. 2017. Younger Dryas glaciers and climate in the Mourne Mountains, Northern Ireland. *Journal of Quaternary Science* **32**: 104-115.

Barnhardt WA, Belknap DF, Kelley JT. 1997. Stratigraphic evolution of the inner continental shelf in response to late Quaternary relative sea-level change, northwestern Gulf of Maine. *Geol. Soc. Am. Bull*. **109**: 612-630.

Bradley SL, Milne GA, Shennan I, Edwards R. 2011. An improved Glacial Isostatic Adjustment model for the British Isles. *Journal of Quaternary Science* **26**: 541-552.

Brooks AJ, Bradley SL, Edwards RJ, Milne GA, Horton B, Shennan I. 2008. Postglacial relative sea-level observations from Ireland and their role in glacial rebound modelling. *Journal of Quaternary Science* **23**: 175-192.

Brooks AJ, Edwards RJ. 2006. The Development of a Sea-Level Database for Ireland. *Irish Journal of Earth Science* **24**: 13-27.

Brutsché KE, Rosati J, Pollock CE, McFall BC. 2016. Calculating Depth of Closure Using WIS Hindcast Data. US Army Corps of Engineers Report ERDC/CHL CHETN-VI-45.

Carter RWG. 1982. Sea-level changes in Northern Ireland. *Proceedings of the Geologists' Association* **93**: 7-23.

Carter RWG, Devoy RJN, Shaw J. 1989. Late Holocene sea levels in Ireland. *Journal of Quaternary Science* **4**: 7-24.

Catuneanu O. 2006. *Principles of Sequence Stratigraphy.* Elsevier.

Chiverrell RC, Thrasher IM, Thomas GSP, Lang A, Scourse JD, van Landeghem KJJ, McCarroll D, Clark CD, Ó Cofaigh C, Evans DJA, Ballantyne CK. 2013. Bayesian modelling the retreat of the Irish Sea Ice Stream. *Journal of Quaternary Science* **28**: 200–209.

Clark CD, Ely JC, Greenwood SL, Hughes ALC, Meehan R, Barr ID, Bateman MD, Bradwell T, Doole J, Evans DJA, Jordan CJ, Monteys X, Pellicer XM, Sheehy M. 2018. BRITICE Glacial Map, version 2: a map and GIS database of glacial landforms of the last British–Irish Ice Sheet. *Boreas* **47**: 11-e8.

Davis RA, Dalrymple RW. 2012. *Principles of Tidal sedimentology.*

Devoy RJ. 1983. Late Quaternary shorelines in Ireland: an assessment of their implications for isostatic land movement and relative sea-level changes. In *Shorelines and Isostasy*, Smith DE, Dawson AG (eds). Academic Press, London: 227-254.

Devoy RJN. 1991. The study of inferred patterns of Holocene sea-level change from Atlantic and other European coastal margins as a means of testing models of Earth crustal behaviour. In *Glacial Isostasy, Sea-level and Mantle Rheology*, Sabadini R, Lambeck, K, Boschi, E (eds). Kluwer Academic Publishers, Dordrecht: 213-236.

Edwards R, Brooks A, Shennan I, Milne G, Bradley S. 2008. Reply: postglacial relative sea-level observations from Ireland and their role in glacial rebound modelling. *Journal of Quaternary Science* **23**: 821-825.

Edwards R, Craven K. 2017. Relative Sea-Level Change Around the Irish Coast. In *Advances in Irish Quaternary Studies,* Coxon P, McCarron S, Mitchell F (eds.) Atlantis Press: 181-215.

Finlayson A, Fabel D, Bradwell T, Sugden D. 2014. Growth and decay of a marine terminating sector of the last British Irish Ice Sheet. *Quaternary Science Reviews* **83**: 28–45.

Gray JM, Coxon, P. 1991. The Loch Lomond Stadial Glaciation in Britain and Ireland. In *Glacial deposits in Britain and Ireland*, Ehlers J, Gibbard PL, Rose L (eds). A.A. Balkema, Rotterdam: 89-105.

Judd AG, Hovland M. 1992. The evidence of shallow gas in marine sediments. *Continental Shelf Research* **12**: 1081-1095.

Kelley JT, Cooper JAG, Jackson DWT, Belknap DF, Quinn RJ. 2006. Sea-level change and inner shelf stratigraphy off Northern Ireland. *Marine Geology* **232**: 1-15.

Kuchar J, Milne G, Hubbard A, Patton H, Bradley S, Shennan I, Edwards R. 2012. Evaluation of a numerical model of the British–Irish ice sheet using relative sea-level data: implications for the interpretation of trimline observations. *Journal of Quaternary Science* **27**: 597-605.

Lambeck K, Rouby H, Purcell A, Sun Y, Sambridge M. 2014. Sea level and global ice volumes from the last glacial maximum to the Holocene. *Proceedings of the National Academy of Sciences* U. S. A. **111:** 15296-15303.

Lamplugh GW, Kilroe JR, M'Henry A, Seymour HJ, Muff HB, Wright WB. 1904. *The geology of the Country around Belfast: Explanation of the Belfast colour-printed drift map.* HMSO, Dublin.

Lisitzin AP. 2002. *Sea-Ice and Iceberg Sedimentation in the Ocean: Recent and Past.* Springer.

Liu JP, Milliman JD. 2004. Reconsidering melt-water pulses 1A and 1B: Global impacts of rapid sea-level rise. *Journal of Ocean University of China* **3**: 183-190.

Manning PI, Robbie JA, Wilson HE. 1970. *Geology of Belfast and the Lagan Valley*. Memoirs of the Geological survey, Northern Ireland. HMSO, Belfast.

McCabe AM. 2008. Comment: postglacial relative sea-level observations from Ireland and their role in glacial rebound modelling. A. J. Brooks, S. L. Bradley, R. J. Edwards, G. A. Milne, B. Horton and I. Shennan (2008). Journal of Quaternary Science 23: 175-192. *Journal of Quaternary Science* **23**: 817-820.

McCabe AM, Clark PU. 1998. Ice sheet variability around the North Atlantic Ocean during the last deglaciation. *Nature* **392**: 373-377.

McCabe AM, Cooper JAG, Kelley JT. 2007. Sea-level changes from NE Ireland during the last glacial termination. *Journal of the Geological Society, London* **164**: 1059-1063.

McCabe AM, Williams GD. 2012. Timing of the East Antrim Coastal Readvance: phase relationships between lowland Irish and upland Scottish ice sheets during the last glacial termination. *Quaternary Science Reviews* **58**: 18–29.

Nicholls RJ, Larson M, Copobianco M, Birkemeier WA. 1998. Depth of closure: Improving understanding and prediction. *Proceedings, Coastal Engineering* **1998**: 2888- 2901.

Oldale RN, Knebel HJ, Bothner MH. 1994. Submerged and eroded drumlins off northeastern Massachusetts. *Geomorphology* **9**: 301-309.

Ortiz AC, Ashton AD. 2016. Exploring shoreface dynamics and a mechanistic explanation for a morphodynamic depth of closure. *Journal of Geophysical Research: Earth Surface* **121**: 442–464.

Poirier C, Sauriau P-G, Chaumillon E, Allard J. 2009. Can molluscan assemblages give insights into Holocene environmental changes other than sea-level rise? A case study from a macrotidal bay (Marennes-Oleron, France). *Palaeogeography, Palaeoclimatology, Palaeoecology* **280**: 105-118.

Rasmussen SO, Andersen KK, Svensson AM, Steffensen JP, Vinther BM, Clausen HB, Siggaard-Andersen ML, Johnsen SJ, Larsen LB, Dahl-Jensen D, Bigler M, Röthlisberger R, Fischer H, Goto-Azuma K, Hansson ME. Ruth U. 2006. A new Greenland ice core chronology for the last glacial termination. *Journal of Geophysical Research* **111**: D06102.

Scourse JD, Ward SL, Wainwright A, Bradley SL, Uehara, K. 2018. The role of megatides and relative sea level in controlling the deglaciation of the British–Irish and Fennoscandian ice sheets. *Journal of Quaternary Science* **33**: 139-149.

Shaw J, Fader GB, Taylor RB. 2009. Submerged early Holocene coastal and terrestrial landforms on the inner shelves of Atlantic Canada. *Quaternary International* **206**: 24-34.

Yokoyama Y, Esat TM, Thompson WG, Thomas AL, Webster JM, Miyairi Y, Sawada C, Aze T, Matsuzaki H, Okuno J, Fallon S, Braga J-C, Humblet M, Iryu Y, Potts DC, Fujita K, Suzuki A, Kan H. 2018. Rapid glaciation and a two-step sea level plunge into the Last Glacial Maximum. *Nature* **559:** 603–607.

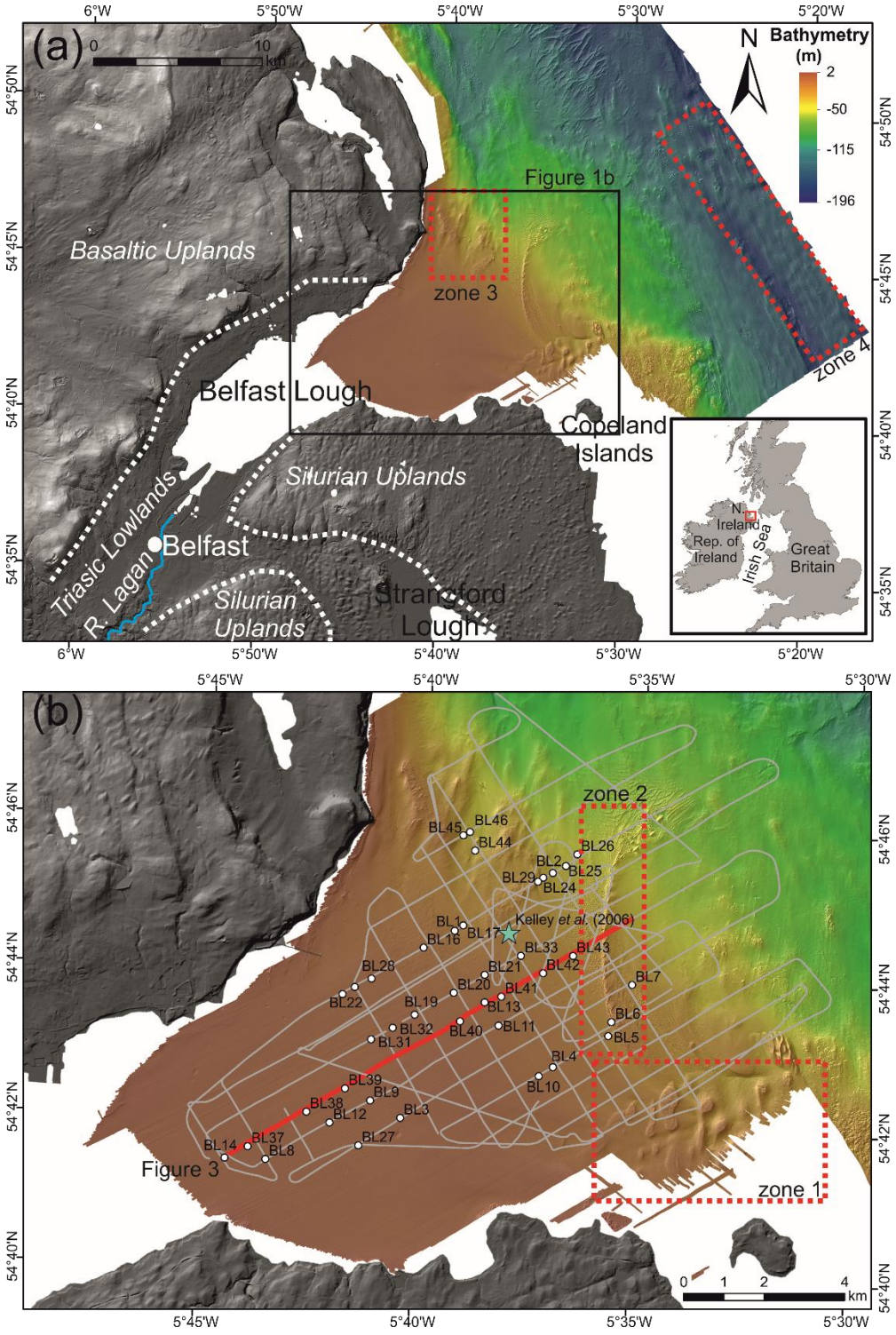

Figure 1. Location of the study area. (a) Multibeam data of the offshore region and onshore digital elevation model, with a broad overview of the underlying bedrock. (b) Detailed map showing the core sampling locations and acquired seismic data; blue star shows location of the core described by Kelley et al. (2006); red line shows pinger line illustrated in Figure 3. Zones 1-4 are geomorphological features discussed in the text.

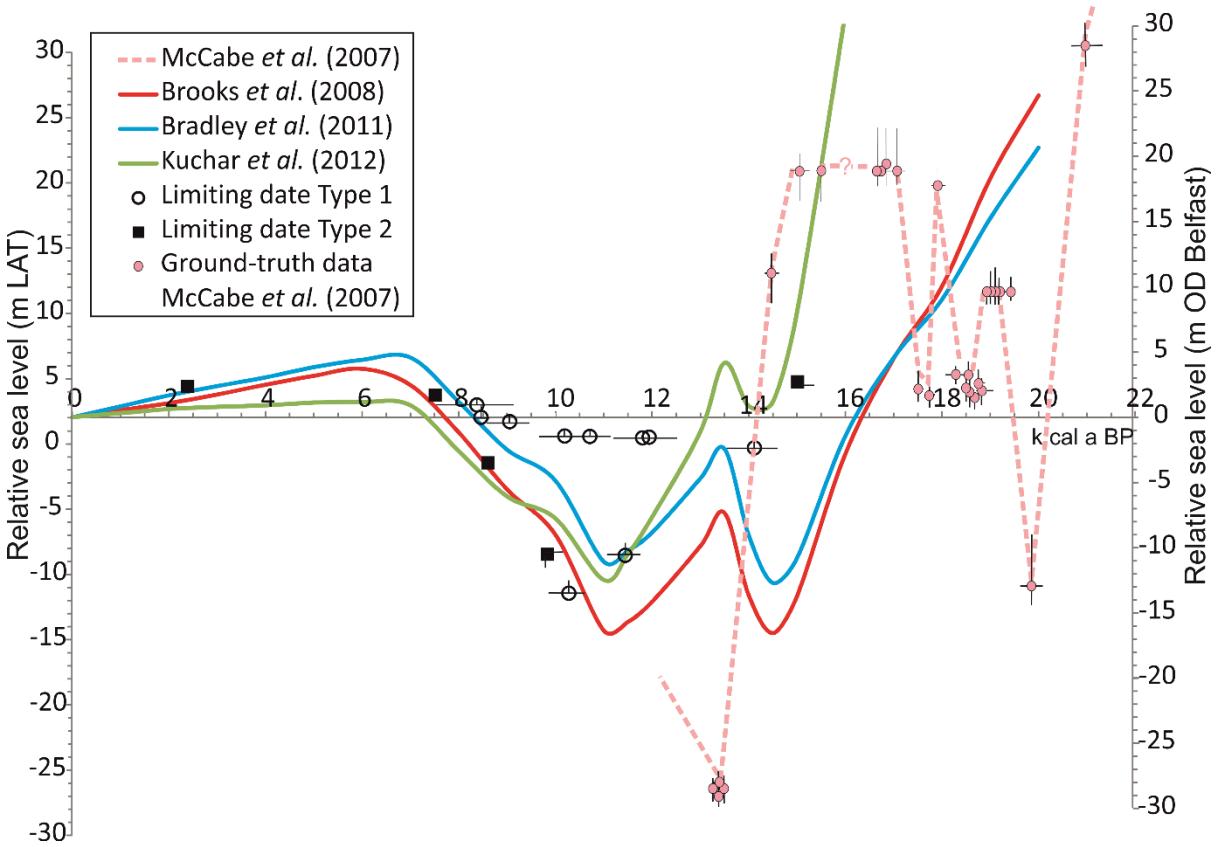

Figure 2. Three recent GIA model-derived RSL curves (Brooks et al., 2008 (Model E); Bradley et al., 2011; Kuchar et al., 2012) and McCabe et al.'s (2007) reconstruction with limiting sea-level index points extracted from Brooks and Edwards' (2006) database. Limiting date type 1 points have a known age and environment but no quantifiable sea level position; limiting date type 2 points contain material whose source environment is contested or unclear. OD Belfast refers to mean sea level; LAT refers to lowest astronomical tide (2 m below mean sea level).

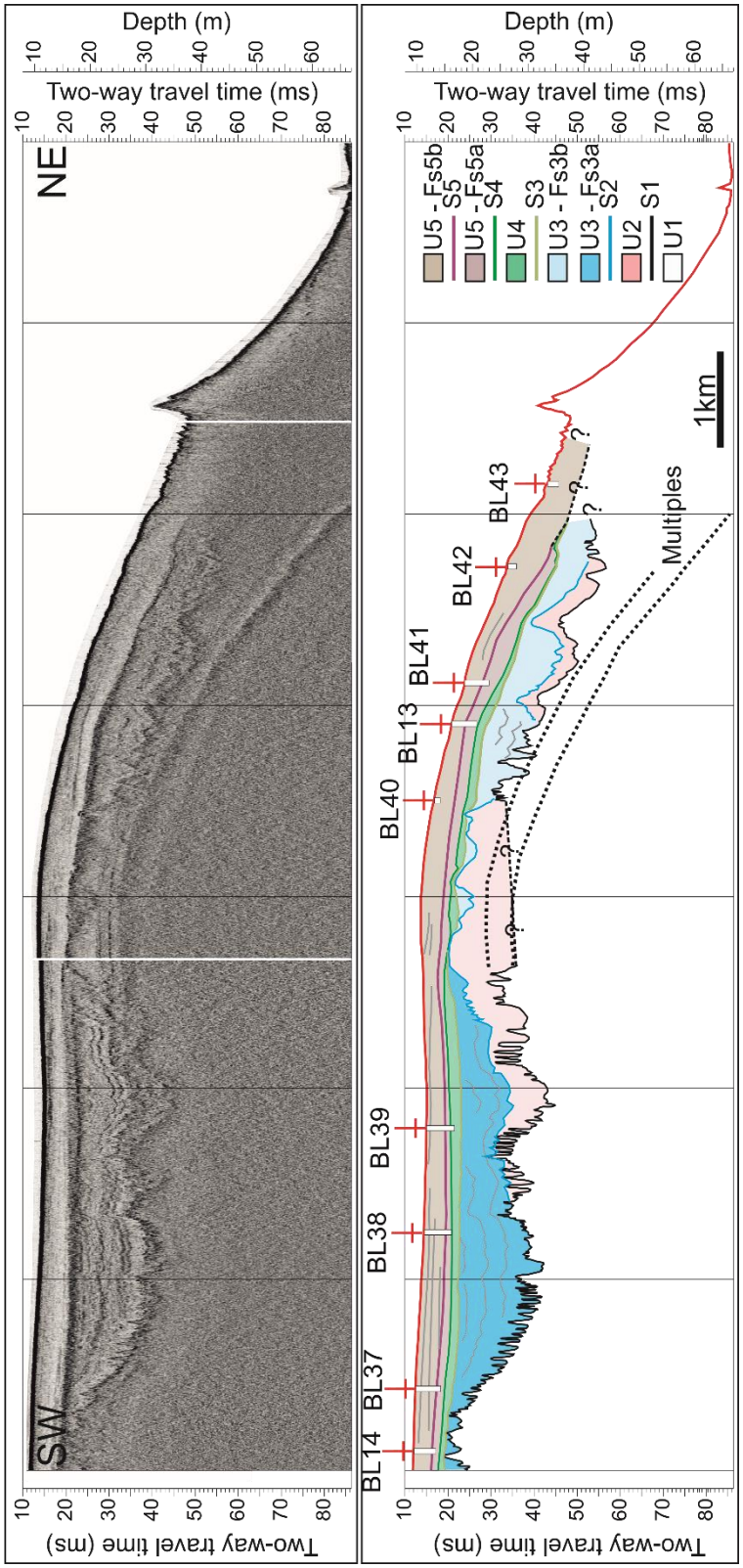

Figure 3. Interpreted seismic Pinger line showing core locations. For position of the line, see figure 1b; for the description of the seismic facies, see Table 1.

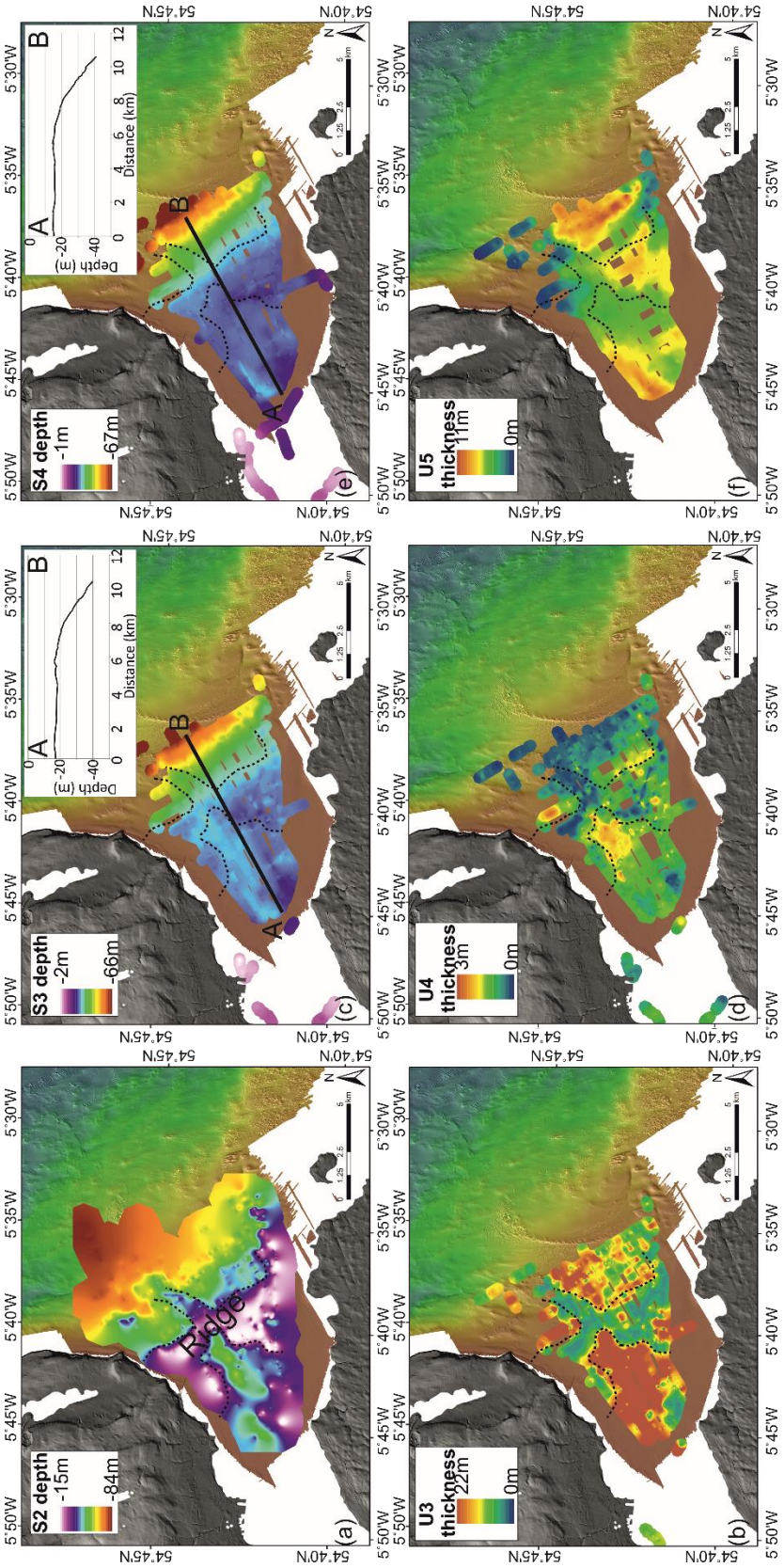

Figure 4. Interpolated and gridded depths of the main unconformities S2 (a), S3 (c) and S4 (e) with profiles lines for the latter two, and thickness maps of seismic units U3 (b), U4 (d) and U5 (f). The dotted line outlines the location of a raised ridge system dividing the Lough into the inner basin and the outer Lough.

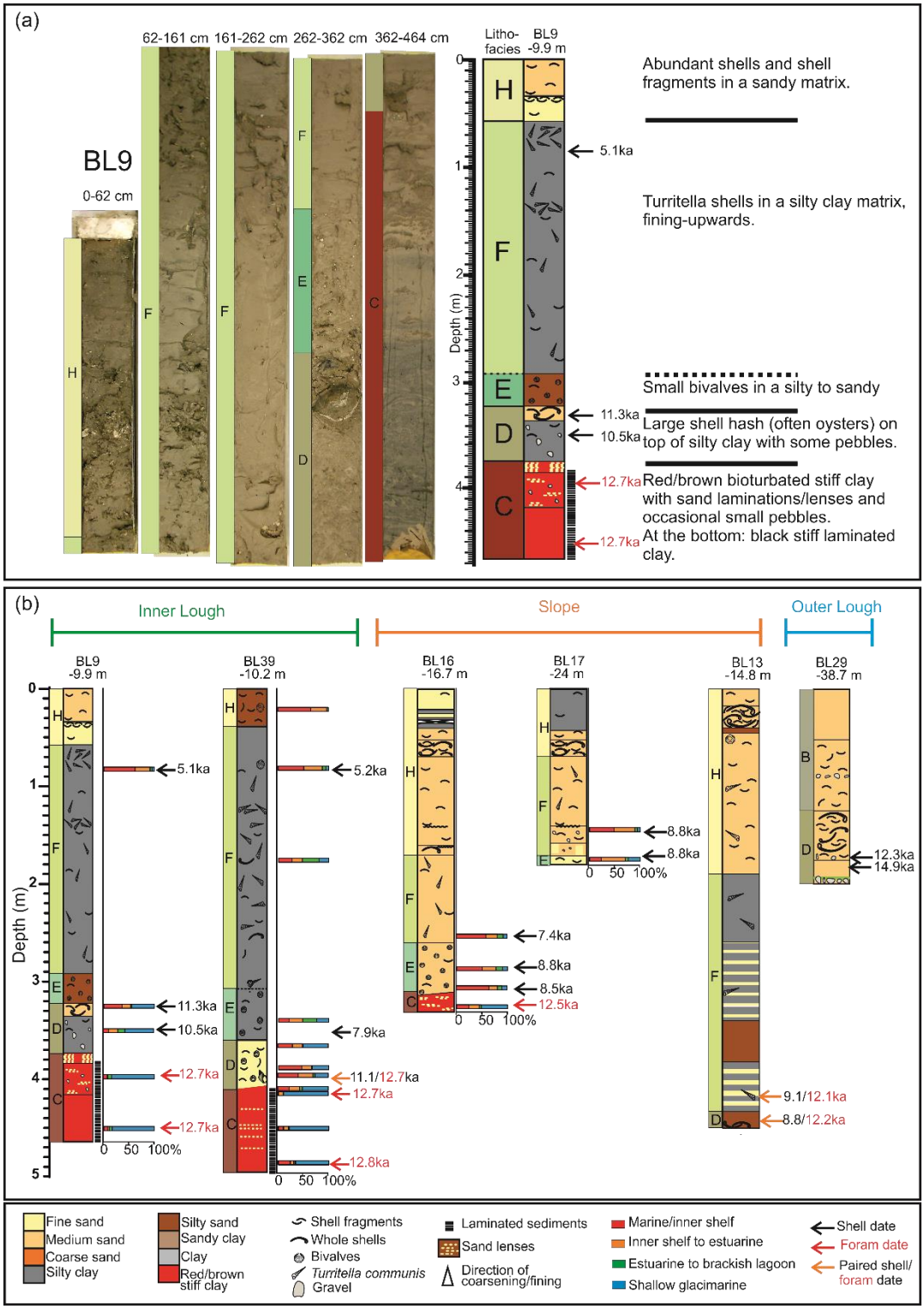

Figure 5. (a) Typical core collected from the inner Lough with the description, assigned lithofacies and dated samples. (b) Transect of cores for which radiocarbon dates were acquired, together with lithofacies interpretation and relative palaeo-environmental abundance of foraminifera. For the location of the cores, see Figure 1b.

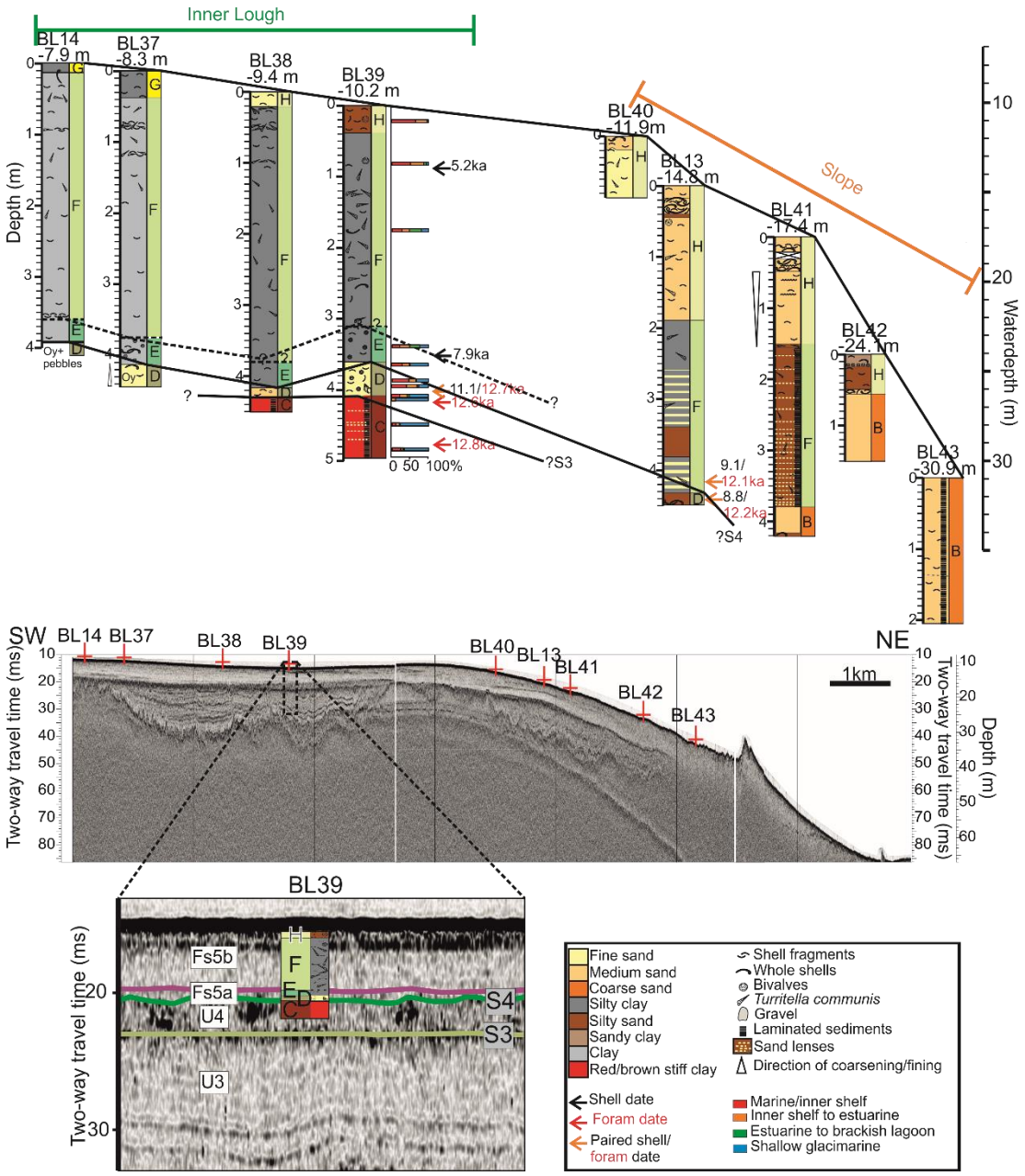

Figure 6. Core stratigraphy along the Lough and correlation with the seismic data. For the location of the seismic line and cores, see Figure 1b. Core BL39 has been selected as a representative core for the inner Lough to correlate the seismo- and lithostratigraphy.

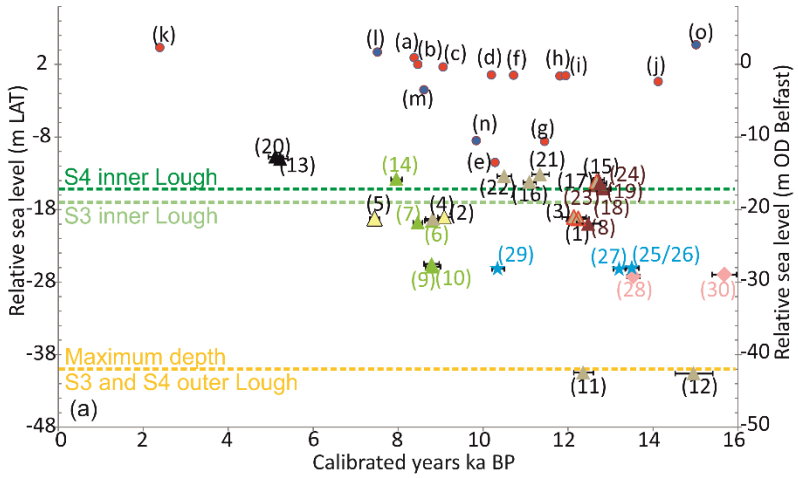
S4 inner Lough
S3 inner Lough
Maximum depth
S3 and S4 outer Lough
(a)
Relative sea level (m LAT)
Relative sea level (m OD Belfast)
Calibrated years ka BP

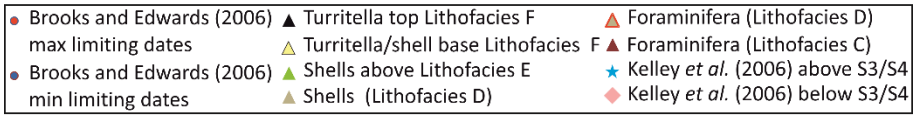
Brooks and Edwards (2006) max limiting dates
Brooks and Edwards (2006) min limiting dates
Turritella top Lithofacies F
Turritella/shell base Lithofacies F
Shells above Lithofacies E
Shells (Lithofacies D)
Foraminifera (Lithofacies D)
Foraminifera (Lithofacies C)
Kelley et al. (2006) above S3/S4
Kelley et al. (2006) below S3/S4

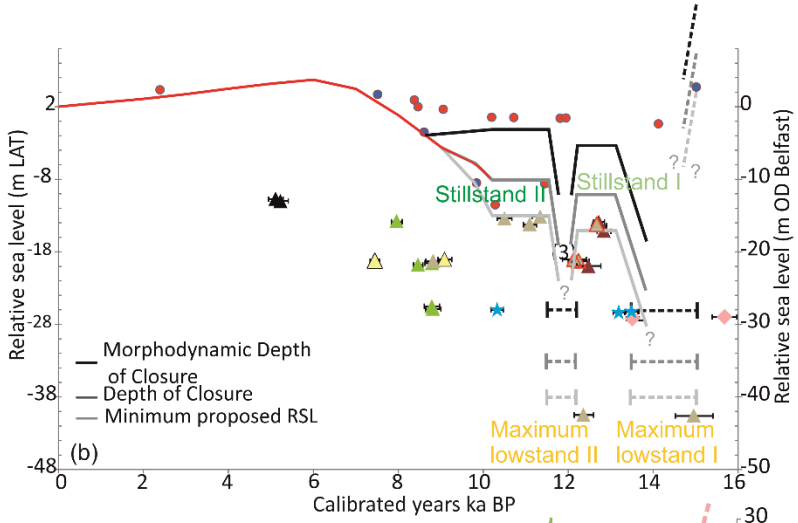
Stillstand II
Stillstand I
Morphodynamic Depth of Closure
Depth of Closure
Minimum proposed RSL
Maximum lowstand II
Maximum lowstand I
(b)
Relative sea level (m LAT)
Relative sea level (m OD Belfast)
Calibrated years ka BP

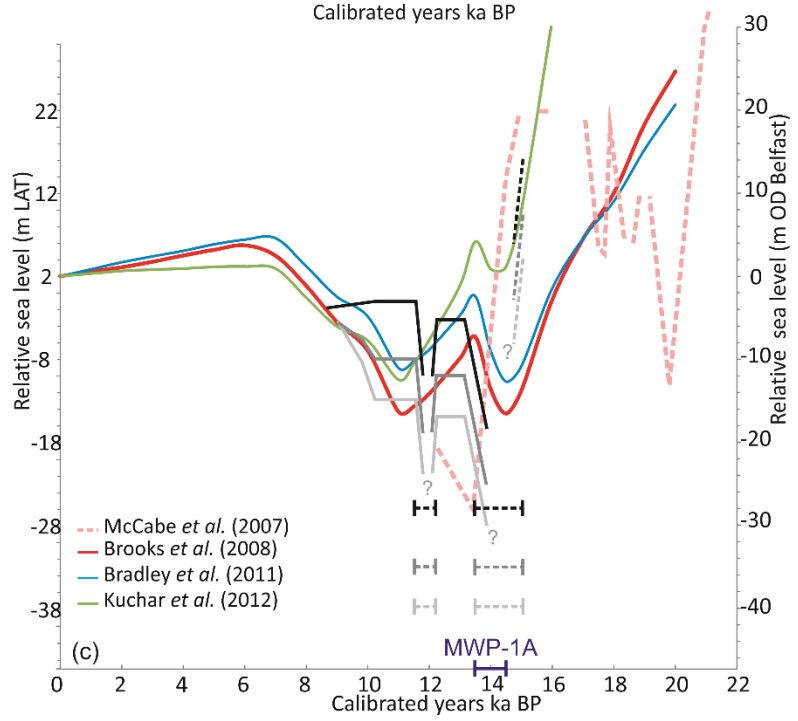
McCabe et al. (2007)
Brooks et al. (2008)
Bradley et al. (2011)
Kuchar et al. (2012)
MWP-1A
(c)
Relative sea level (m LAT)
Relative sea level (m OD Belfast)
Calibrated years ka BP

Figure 7. (a) Summary plot of limiting dates (Brooks et al., 2008) and marine radiocarbon dates described in this paper. The bracketed numbers refer to the radiocarbon samples as numbered in Table 2. No y-axis terms are defined – depths were defined from MBES depths projected using core coordinates – we estimate a maximum vertical error of +/- 5 m. (b) Radiocarbon dates combined with a proposed minimum relative sea level curve (light grey); the Depth of closure (dark grey) and Morphodynamic Depth of Closure (black) are annotated. (c) Comparison of the proposed relative minimum, DoC and MDoC sea-levels curve with GIA model derived reconstructions (Brooks et al., 2008; Bradley et al., 2011; Kuchar et al., 2012) and McCabe et al.'s (2007) reconstruction. The purple bar illustrates the interval between 14.5 and 13.5k cal a BP during which MWP-1A is introduced in the GIA model approach.

Table 1. Description and interpretation of the seismic facies, with corresponding lithofacies.

Seismic Unit	Seismic Facies	Boundary surface	Pinger envelope	Continuity	Amplitude	Frequency	Configuration	Lower reflection terminations	Upper reflection terminations	Corresponding lithofacies	Interpretation
U5	Fs5b		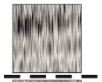	Mostly continuous	Medium	Medium	(Sub)parallel	Conformable/ onlap	Conformable	Lithofacies F, G & H	Fully marine
	Fs5a			Mostly continuous	Low	Medium	(Sub)parallel	Conformable	Conformable	Lithofacies E& D	Estuarine
		S4		Disrupted	High						
U4	Fs4			Dis-continuous	High	Medium to high	Contorted to chaotic	Onlap/ downlap	Truncation	Lithofacies C	Gas/organic-rich sediments
		?—?S3		Mostly dis-continuous	Medium to high						
U3	Fs3b (Outer Lough)			Dis-continuous	Medium	Medium	Contorted to chaotic	Onlap	Conformable?/ truncation	Lithofacies A & I	Reworked glacial sediment/ glacimarine
	Fs3a (Inner Lough)			Continuous	High	High	Wavy, parallel	Onlap	Truncation	Not cored	Glacilacustrine/ glacimarine
		S2		Mostly dis-continuous	Low to medium						
U2	Fs2			Dis-continuous	Low	Medium	Disrupted	Onlap	Truncation	Not cored	Till (LGM/ re-advance?)
		S1		Mostly dis-continuous	High						
U1	Fs1			Dis-continuous	Medium	Medium	Chaotic	-	Truncation	Not cored	Basement

Table 2. Selected species and depths for radiocarbon dating

No	**Core**	Lab code	**Sample depth (cm)**	**Total depth (m below LAT)**	**Lithofacies**	**Species dated**	**$d^{13}C$**	**^{14}C Age yrs BP ± 1σ)**	**Calibrated age: median probability yrs BP**	**Calibrated age: mean (Marine13) yrs BP ± 2SD**
1	BL13	SUERC-45964	420-421	19.0-19.01	F	Foraminifera *(Quinqueloculina seminulum)*	0.3	10647 ± 62	12083	12118 ± 291
2	BL13	SUERC-45951	420-421	19.0-19.01	F	Marine shell *(Abra sp.)*	1.0	8392 ± 60	9051	9067 ± 184
3	BL13	SUERC-45962	440-441	19.2-19.21	D	Foraminifera *(Quinqueloculina seminulum)*	0.3	10714 ± 63	12212	12226 ± 259
4	BL13	SUERC-45952	440-441	19.2-19.21	D	Marine shell *(Abra sp.)*	1.4	8245 ± 66	8835	8811 ± 192
5	BL16	SUERC-51625	252-253	19.22-19.23	F	Shell *(Turritella communis)*	3.5	6887 ± 61	7441	7437 ± 117
6	BL16	SUERC-51626	285-286	19.55-19.56	E	Shell *(Corbula gibba)*	1.2	8202 ± 60	8779	8780 ± 185
7	BL16	SUERC-51627	305-306	19.75-19.76	E	Shell (*Corbula gibba)*	1.5	7941 ± 59	8446	8455 ± 118
8	BL16	UCIAMS-139024	324-325	19.94-19.95	C	Foraminifera *(Elphidium excavatum forma clavatum)*	2.2	10970 ± 110	12535	12455 ± 288
9	BL17	SUERC-51630	143-144	25.43-24.44	D	Shell *(Corbula gibba)*	1.8	8199 ± 59	8775	8778 ± 184

10	BL17	SUERC-51631	175-176	25.75-25.76	D	Shell *(Corbula gibba)*	1.5	8232 ± 59	8821	8805 ± 180
11	BL29	SUERC-45950	176-177	40.46-40.47	D	Marine shell *(Abra sp.)*	0.3	10819 ± 63	12378	12340 ± 235
12	BL29	SUERC-46370	185-186	40.55-40.56	D	Marine shell *(Tellina sp)*	-8.5	13022 ± 103	15027	14914 ± 458
13	BL39	SUERC-51633	81-82	11.01-11.02	F	Shell *(Turritella communis)*	3.4	4859 ± 58	5219	5217 ± 189
14	BL39	SUERC-51632	355-356	13.75-13.76	E	Shell *(Corbula gibba)*	1.9	7436 ± 58	7940	7945 ± 136
15	BL39	SUERC-45961	394-400	14.14-14.2	D	Foraminifera *(Elphidium albiumbilicatum)*	-0.4	11107 ± 64	12657	12666 ± 112
16	BL39	SUERC-45953	394-400	14.14-14.2	D	Marine shell *(Abra sp.)*	0.7	10060 ± 62	11108	11077 ± 159
17	BL39	SUERC-48869	415-416	14.35-14.36	C	Foraminifera *(Elphidium excavatum forma clavatum)*	0.4	11088 ± 64	12646	12654 ± 111
18	BL39	UCIAMS-139025	445-446	14.65-14.66	C	Foraminifera *(Elphidium excavatum forma clavatum)*	0.9	11050 ± 64	12623	12627 ± 112
19	BL39	UCIAMS-139026	489-490	15.09-15.1	C	Foraminifera *(Elphidium*	2.5	11320 ± 64	12825	12829 ± 161

						excavatum forma clavatum)				
20	BL9	SUERC-51636	82-83	10.72-10.73	F	Shell *(Turritella communis)*	3.4	4766 ± 59	5101	5093 ± 184
21	BL9	SUERC-51634	325-332	13.15-13.22	D	Shell *(Artica islandica*)	1.9	10219 ± 60	11258	11303 ± 188
22	BL9	SUERC-51635	350-351	13.4-13.41	D	Shell *(Circomphalus casina)*	-0.4	9570 ± 60	10496	10475 ± 178
23	BL9	UCIAMS-139027	398-400	13.88-13.89	C	Foraminifera *(Elphidium excavatum forma clavatum)*	0.0	11165 ± 64	12697	12710 ± 127
24	BL9	UCIAMS-139028	450-451	14.4-14.41	C	Foraminifera *(Elphidium excavatum forma clavatum)*	-1.7	11215 ± 61	12735	12748 ± 133
25	Kelley et al., 2006; BL3	203000	153	26.0	D	Shell *(Mytilis sp)*		11670 ± 61	13204	13206 ± 136
26	Kelley et al., 2006; BL3	202999	153	26.0	D	Shell *(Balanus sp)*		12000 ± 61	13488	13503 ± 163
27	Kelley et al., 2006; BL3	202998	153	26	A?	Shell *(Nuncula sp)*		11990 ± 61	13477	13492 ± 161
28	Kelley et al., 2006; BL4	203001	255	27	I	Shell *(Spisula sp)*		12030 ± 61	13521	13532 ± 166

29	Kelley et al, unpublished; BL3	UB9217	130-140	25.8	E	Shell (infaunal, unidentified)		9437 ± 55	10331	10345 ± 140
30	Kelley et al, unpublished; BL3	UB9216	225	26.7	I	Shell *(Portlandia arctica)*		13449 ± 72	15695	15667.5 ± 292.5

Supplementary information

Methodology

High-resolution seismic data were collected, onboard *RV Celtic Voyager*, with an SES 5000 (3.5 kHz) hull-mounted Pinger system (200 ms pulse length). All data were recorded in CODA and imported into SMT Kingdom 8.8 software for processing and interpretation. This processing included: tidal correction to lowest astronomical tide (LAT), Bandpass filter (2700– 3000–5500–6000Hz), automatic gain control (10ms) and envelope application. Where reflectors and surfaces were gridded, a Flex Gridding algorithm was used with a 10 x 10 m cell size. Core logs were superimposed onto the seismic data using a linear velocity model of 1550 – 1700 m/s over a core length of 6 m. To convert the two-way travel time, an average acoustic velocity of 1600 m/s was assumed

Multibeam bathymetric data were acquired by the Royal Navy and the Agri-Food and Biosciences Institute in 2009 using an EM1002 and EM3002. All data were supplied in processed form at 2 m resolution, referenced to LAT.

Based on the seismic data acquired in 2011, a subsequent cruise on 17th and 18th June 2012 onboard the *RV Celtic Explorer* collected 39 vibrocores, using a 6m long Geo-Vibrocorer (6m barrel, 11cm diameter PVC liner). The recovery of sediment ranged from 0.86 to 5.24 m, in water depths ranging from -7.8 to -54.4 m LAT. Cores were stored horizontally in refrigerated facilities (4°C) after disembarkation. They were split, photographed and described (lithology, texture, contacts, sedimentary structures and Munsell colour). Twenty-four samples were dated using accelerator mass spectrometry (AMS) radiocarbon dating from stratigraphically significant horizons from six cores. Target material included whole bivalves, gastropods or monospecific benthic foraminifera samples. Monospecifc foraminifera samples were wet sieved using 500 and 63 μm sieves. Foraminifera in the fine fraction were wet picked, identified, and dried in an oven at 40 °C. The shell samples were washed in deionised water and dried at 40 °C. Samples with the prefix SUERC were analysed at the SUERC Radiocarbon Dating Laboratory at East Kilbride, with five small samples of monospcific *Elphidium excavatum forma clavatum* sent to Keck C cycle AMS Lab, University of California (prefix UCAIMS). The conventional ages were calibrated using the Marine13 curve (Calib v.7.04, Reimer *et al*., 2013), and corrected for the local reservoir effect of δR of − 45 ± 46 (based on Blake, 2005). Dates are reported as mean (2 sigma range) calibrated calendar years before present (cal a BP) (Table 2). A further twenty-two foraminifera samples from four cores were analysed for assemblage counts. Where possible, a minimum of 300 benthic foraminifera were handpicked from a 3 cc volume of sample, although foraminifera concentrations were too low for the 300-minimum count in some samples (minimum number counted being 117 specimens). Identifications were based on various taxonomic references (e.g. Haynes, 1973, Murray, 1971, Murray, 1979, Murray, 2003, Murray, 1991, Nooijer *et al*., 2008). Whilst benthic and planktonic species were counted, only benthic species were used for percentage calculations.

Supplementary Table 1. Detailed foraminifera analysis; red: marine/inner shelf species, orange: inner shelf to estuarine species, green: estuarine to brackish lagoon species, blue: shallow glacimarine species.

Core	BL39	BL39	BL39	BL39	BL39	BL39	BL39	BL39	BL39	BL39	BL39	BL39
Depth (cm	20-21	80-81	175-176	340-341	365-366	389-390	393-394	409-410	411-412	413-414	450-451	484-485
Lithofacies	H	F	F	E	D	D	D	D	C	C	C	C
Adelosina type	0.2	0.0	0.5	0.7	0.0	2.9	2.3	3.5	0.3	0.0	0.5	0.0
Ammonia batavus	29.3	4.7	1.4	1.4	0.3	0.0	1.0	0.3	0.0	0.0	0.0	0.6
Asterigerinata mamilla	5.5	11.0	3.6	2.1	1.0	1.6	2.0	0.9	1.3	0.5	0.0	0.0
Brizalina difformis	0.5	0.3	0.5	0.0	0.0	0.0	0.0	0.0	0.0	0.0	0.0	0.0
Brizalina variabilis	0.5	3.3	0.2	0.0	0.0	0.4	0.0	0.0	0.8	0.0	0.0	0.0
Bulimina type	2.1	2.1	5.2	4.6	6.0	6.6	2.6	0.9	2.1	0.0	0.0	0.0
Cyclogyra involvens	0.2	0.0	0.0	0.0	0.0	0.0	0.0	0.0	0.0	0.0	0.0	0.0
Elphidium crispum	0.2	0.0	0.0	0.0	0.0	0.0	0.3	0.3	0.0	0.0	0.0	0.0
Elphidium gerthi	9.0	6.8	5.2	3.9	9.6	16.5	15.7	5.4	7.2	0.0	0.0	0.0
Elphidium incertum	0.2	1.2	0.7	1.1	1.0	2.1	2.3	2.5	0.5	0.0	1.4	2.3
Elphidium margaritaceum	1.0	2.1	0.2	1.8	2.0	3.7	4.6	1.3	1.6	0.0	0.0	0.0
Fissurina lucida	0.2	2.4	0.2	0.4	0.3	1.6	2.0	0.0	0.5	0.5	0.0	0.0
Fissurina marginata	1.4	0.6	0.0	0.0	0.0	0.0	0.0	0.0	0.0	0.0	0.0	0.0
Lagena striata	0.2	0.6	0.0	0.0	0.0	0.0	0.0	0.0	0.0	0.0	0.0	0.0
Nonionella turgida	0.0	1.5	0.5	1.1	0.3	0.0	0.0	0.0	0.3	0.0	0.0	0.0
Nonionella type	0.5	0.0	0.7	0.0	0.0	0.0	0.0	0.0	0.0	0.0	0.0	0.0
Oolina melu	0.2	0.0	0.0	0.0	0.0	0.0	0.0	0.0	0.0	0.0	0.0	0.0
Oolina williamsoni	1.6	0.0	0.7	0.0	0.7	0.4	0.3	0.0	0.3	0.0	0.0	0.0

Patellina corrugata	3.4	2.4	0.0	0.0	0.7	0.0	0.0	0.0	0.0	0.0	0.0	0.0
Procerolagena clavata	0.2	0.0	0.5	0.4	0.0	0.4	0.0	0.0	0.5	0.0	0.0	0.0
Pyrgo elongata	0.0	0.0	0.2	0.7	0.3	0.4	0.3	0.3	0.3	0.0	1.9	11.6
Pyrgo williamsoni	0.0	0.3	0.5	0.0	0.0	0.8	0.0	0.0	1.1	1.1	3.8	8.1
Quinqueloculina type	5.5	6.8	3.1	3.2	6.3	11.1	7.8	7.3	10.7	0.5	3.3	1.7
Rosalina anomala	1.4	8.0	1.9	0.4	1.3	0.0	1.0	0.0	0.8	0.0	0.0	0.0
Spirulina vivipara	0.0	1.5	1.2	0.7	0.0	0.4	0.0	0.0	0.0	0.0	1.9	0.6
Spiroloculina type	0.0	0.0	0.0	0.0	0.0	0.0	0.0	0.3	0.8	0.0	0.0	0.0
Stainforthia fusiformis	0.0	1.2	0.2	0.0	0.3	0.0	0.0	0.0	0.0	0.0	0.0	0.0
Textularia sagittula	0.9	0.0	0.5	0.0	0.0	0.0	0.0	0.0	0.0	0.0	0.0	0.0
Textularia truncata	0.0	0.3	0.0	0.0	0.0	0.0	0.0	0.0	0.0	0.0	0.0	0.0
Trifarina angulosa	1.2	0.0	0.0	0.0	0.0	0.4	0.3	0.0	0.0	0.0	0.0	0.0
Trochammina ochrea	0.3	0.0	0.0	0.0	0.0	0.0	0.0	0.0	0.0	0.0	0.0	0.0
Bolivinellina pseudopunctata	0.2	0.6	0.0	0.0	0.3	0.0	0.0	0.0	0.0	0.0	0.0	0.0
Cassidulina laevigata	2.9	0.3	0.0	0.0	0.0	0.4	0.0	0.0	0.0	0.5	0.9	0.6
Cassidulina neoteretis	0.0	0.0	0.0	0.0	0.0	0.0	0.3	0.9	0.5	0.0	0.0	0.0
Cassidulina obtusa	1.4	3.3	0.0	0.0	0.3	0.0	0.0	0.6	0.0	2.2	0.9	1.2
Cibicides lobatulus	18.6	6.5	1.7	0.7	0.7	2.9	15.7	3.5	2.9	2.2	2.3	2.9
Elphidium excavatum	3.1	14.2	14.7	24.8	14.6	7.8	5.9	3.2	1.6	3.3	3.8	0.6
Haynesina depressa	0.0	5.6	0.0	0.0	0.0	0.0	0.3	1.3	0.3	0.0	0.0	0.0
Miliolinella sp	2.2	1.5	1.4	0.7	1.3	5.8	4.6	11.1	10.4	0.0	0.0	1.2

Planorbulina mediterranensis	2.1	0.0	0.9	0.0	1.0	0.0	0.0	0.0	0.5	0.0	0.0	0.0
Elphidium albiumbilicatum	0.0	0.0	0.0	0.4	0.3	0.4	1.3	24.1	14.1	18.0	16.9	15.1
Elphidium excavatum forma clavatum	0.0	5.3	20.1	23.8	49.7	31.7	25.2	27.2	35.5	69.9	61.5	50.6
Nonionella labradorica	0.0	0.0	0.5	0.0	0.0	0.0	0.0	0.0	0.0	0.0	0.0	0.0
Ammonia beccarii type	3.6	3.9	31.5	24.1	1.0	0.4	0.3	1.9	1.3	0.0	0.0	0.0
Elphidium williamsoni	0.3	1.2	0.2	1.1	0.0	0.0	0.7	1.9	1.3	0.5	0.0	0.6
Haynesina germanica	0.0	0.6	1.2	2.1	0.7	1.2	3.3	1.3	2.1	0.5	0.9	2.3

Core	BL9	BL9	BL9	BL9	BL9	BL16	BL16	BL16	BL16	BL17	BL17
Depth (cm)	82-83	325-326	350-351	398-400	450-451	255-256	285-286	305-306	325-326	148-149	175-176
Lithofacies	F	D	D	C	C	F	E	E	C	F	D
Adelosina type	0.3	0.0	0.0	0.0	0.0	0.0	2.0	2.2	0.3	1.1	0.4
Ammonia batavus	2.7	0.9	0.9	0.0	0.0	0.7	0.0	0.0	0.0	0.0	0.4
Asterigerinata mamilla	11.9	0.9	1.7	0.2	0.1	24.6	15.7	19.3	1.2	14.9	2.7
Brizalina difformis	1.8	0.0	0.0	0.0	0.0	2.9	2.5	1.5	0.0	1.1	0.9
Brizalina spathulata	0.0	0.0	0.0	0.0	0.0	0.0	0.0	0.0	0.0	0.8	0.4
Brizalina variabilis	0.3	0.0	0.0	0.0	0.0	0.7	0.0	0.0	0.3	0.4	1.3
Bulimina type	4.3	5.1	0.9	0.1	0.1	0.0	1.0	3.0	1.4	1.9	0.4
Cyclogyra involvens	0.3	0.0	0.0	0.0	0.0	0.0	0.0	0.0	0.5	0.0	0.0
Cyclogyra involvens	0.3	0.0	0.0	0.1	0.2	0.7	0.5	0.7	0.2	0.0	0.0
Elphidium gerthi	5.5	11.1	0.9	0.4	0.1	1.4	2.5	6.7	0.0	3.1	0.9
Elphidium incertum	0.0	6.0	7.7	1.9	1.3	0.0	0.5	0.0	6.2	0.0	1.8

Elphidium margaritaceum	3.0	0.0	0.0	0.1	0.2	0.0	0.0	0.0	0.3	0.0	1.8
Fissurina lucida	0.0	0.0	0.0	0.0	0.0	0.0	1.0	0.0	0.0	0.0	0.4
Fissurina marginata	0.9	0.0	0.0	0.0	0.0	1.4	0.5	0.7	0.2	0.4	0.0
Lagena type	0.0	0.0	0.0	0.2	0.1	0.0	0.5	1.5	0.3	0.0	0.0
Nonionella turgida	0.0	0.0	0.0	0.0	0.0	0.7	0.0	0.0	0.0	0.4	0.0
Oolina melu	0.0	0.0	0.0	0.0	0.0	0.0	0.0	0.0	0.0	0.0	0.9
Oolina williamsoni	0.6	0.0	0.0	0.0	0.2	0.0	2.0	2.2	0.7	0.8	0.0
Patellina corrugata	2.4	0.0	0.0	0.0	0.0	1.4	0.0	0.0	0.0	0.4	0.0
Procerolagena clavata	0.0	0.0	0.0	0.0	0.0	0.0	0.5	0.0	0.2	0.0	0.0
Pyrgo elongata	0.0	0.0	0.0	0.0	0.0	0.7	0.0	0.0	0.0	0.0	0.0
Pyrgo williamsoni	0.6	0.0	0.0	2.8	3.6	0.0	1.5	0.0	4.2	0.4	0.4
Quinqueloculina agglutinus	0.0	0.9	0.0	1.0	0.3	0.7	0.0	0.0	1.6	0.0	0.0
Quinqueloculina sp	6.4	12.0	0.0	1.2	2.7	9.4	8.3	17.0	5.7	8.8	6.6
Rosalina anomala	14.6	0.0	0.0	0.0	0.0	6.5	10.3	8.1	0.2	9.2	2.7
Spirulina vivipara	1.2	0.0	0.0	0.0	0.1	3.6	1.0	0.0	0.0	0.8	0.0
Spiroloculina type	0.0	0.0	0.0	0.0	0.0	0.0	0.0	0.0	0.0	0.0	0.4
Stainforthia fusiformis	1.5	0.0	0.0	0.0	0.0	0.0	0.0	0.0	0.0	0.0	0.0
Textularia sagittula	0.0	0.0	0.0	0.0	0.0	4.3	1.5	1.5	0.0	2.7	0.4
Textularia truncata	3.6	0.0	0.0	0.0	0.0	1.4	3.4	0.0	0.0	1.9	0.4
Trifarina angulosa	0.3	0.0	0.0	0.0	0.0	0.0	0.0	0.0	0.0	0.4	0.0
Bolivinellina pseudopunctata	1.2	0.9	0.0	0.0	0.0	0.0	0.0	0.7	0.3	0.4	0.4
Cassidulina laevigata	0.9	0.0	2.6	0.1	0.0	0.7	0.5	0.0	0.3	1.1	0.4

Cassidulina obtusa	4.0	0.9	1.7	0.3	0.9	0.7	6.4	2.2	1.9	5.7	12.8
Cibicides lobatulus	7.3	0.0	13.7	0.9	1.5	12.3	10.8	4.4	11.8	27.5	25.7
Elphidium excavatum	8.5	6.0	0.0	0.4	0.0	0.0	0.0	0.0	0.0	0.4	1.3
Haynesina depressa	4.6	0.9	0.0	0.0	0.2	0.7	0.0	0.7	0.3	0.0	0.9
Miliolinella sp	2.7	8.5	0.0	0.2	0.2	1.4	5.4	5.2	5.0	3.1	5.3
Planorbulina mediterranensis	1.2	0.0	0.0	0.0	0.0	2.9	2.5	3.0	0.0	3.8	0.4
Elphidium albiumbilicatum	0.0	0.0	35.9	16.2	10.2	0.0	0.0	0.0	11.8	0.0	1.8
Elphidium excavatum forma clavatum	3.0	44.4	20.5	67.1	72.3	7.2	6.4	10.4	40.7	3.1	21.2
Hyalinea baltica	0.0	0.0	0.0	0.0	0.1	0.0	0.0	0.0	0.0	0.4	0.0
Nonionella labradorica	0.0	0.0	0.0	0.0	0.1	0.0	0.0	0.0	0.0	0.0	0.0
Ammonia beccarii type	3.0	1.7	4.3	0.3	0.4	12.3	12.3	8.9	0.7	5.3	5.3
Elphidium williamsoni	0.6	0.0	0.0	0.0	0.0	0.0	0.5	0.0	0.2	0.0	0.4
Haynesina germanica	0.3	0.0	9.4	6.7	5.3	0.0	0.5	0.0	3.3	0.0	0.4

References

Blake CB. 2005. Use of maerl as a biogenic archive. Unpublished PhD thesis. Biological Sciences, Queen's University Belfast, Belfast.

Haynes JR. 1973. *Cardigan Bay Recent Foraminifera: Cruise of the R.V. Anthur, 1962–1964.* The Bulletin of the British Museum (Natural History) Zoology Supplement.

Murray JW. 1971. *An Atlas of British Recent Foraminids*. Heinemann Educational Books, London.

Murray JW. 1979. *British Nearshore Foraminiferids; key and Notes for the Identification of Species*. Academic Press, London.

Murray JW. 1991. *Ecology and palaeoecology of benthic foraminifera*. Longman Scientific and Technical, New York.

Murray JW. 2003. An illustrated guide to the benthic foraminifera of the hebridean shelf, west of Scotland, with notes on their mode of life. *Palaeontologica Electronica* **5**: 1–31.

Nooijer LJ, Duijnstee IAP, Bergman MJN, van der Zwaan GJ. 2008. The ecology of benthic foraminifera across the Frisian Front, southern North Sea. *Estuarine, Coastal and Shelf Science* **78:** 715–726.

Reimer P, Bard E, Bayliss A, Beck JW, Blackwell PG, Ramsey CB, Buck, H, Cheng H, Edwards RL, Friedrich M, Grootes PM, Guilderson TP, Hafildason H, Hajdas I, Hatté C, Heaton TJ, Hoffman DL, Hogg AG, Hughen KA, Kaiser KF, Kromer B, McCormac FG, Manning SW, Nui M, Reimer RW, Richards DA, Scott EM, Southon JR, Staff RA, Turney CSM, van der Plicht J. 2013. Intcal13 and Marine13 radiocarbon age calibration curves, 0-50,000 years Cal Bp. *Radiocarbon* **55:** 1869-1887.

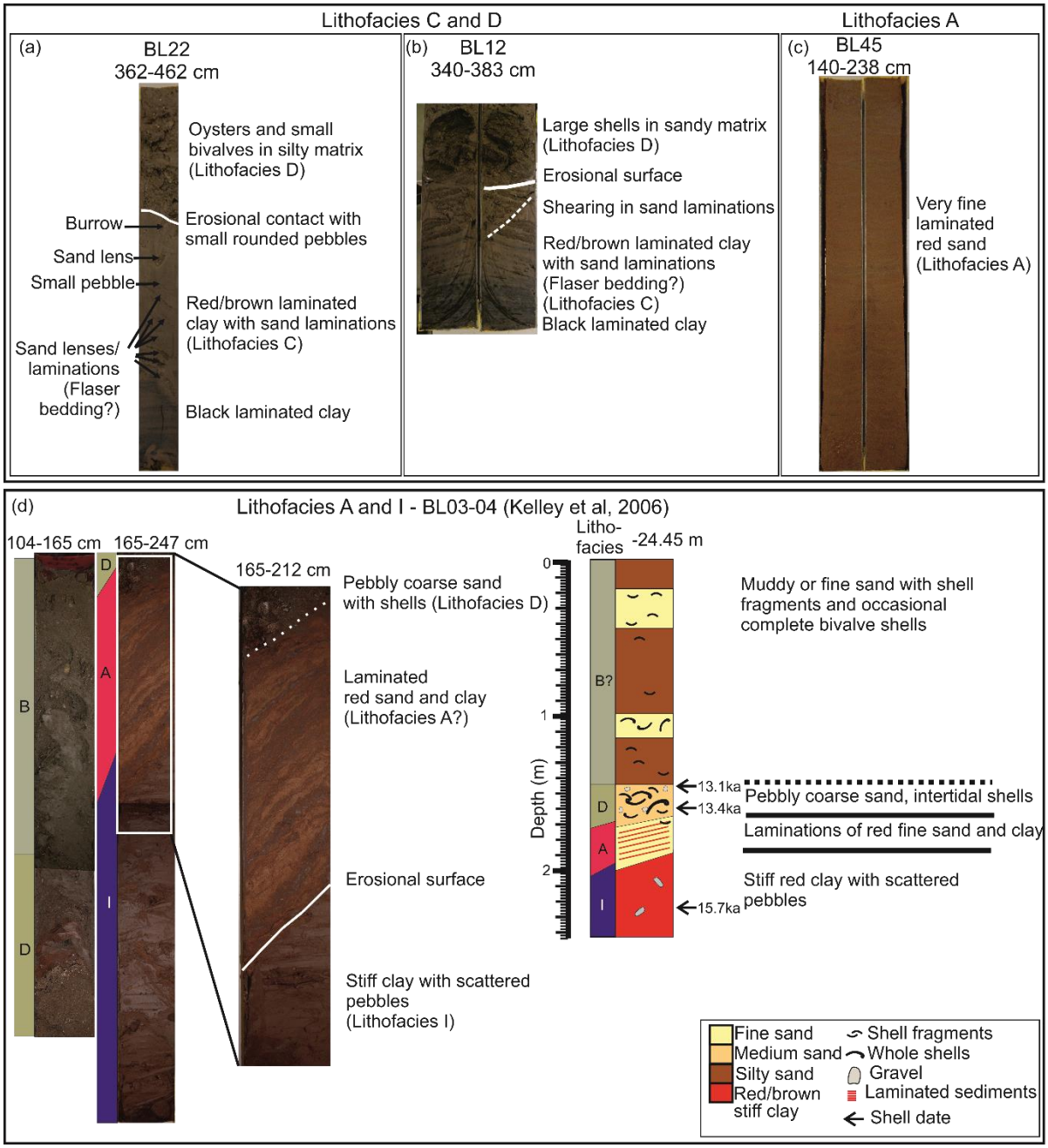

Supplementary Figure S1. Photos showing details of some of the lithofacies. In particular, (a) shows the contrast and erosional contact between Lithofacies C and D as well as the change in colour from black to red/brown throughout lithofacies C; (b) shows the shearing present in Lithofacies C; (c) and (d) illustrate the similarity in colour and the laminated structure of Lithofacies A observed in BL45 and the core described by Kelley et al., (2006). (d) Also shows the core section described by Kelley et al. (2006) with dated samples and interpreted lithofacies.

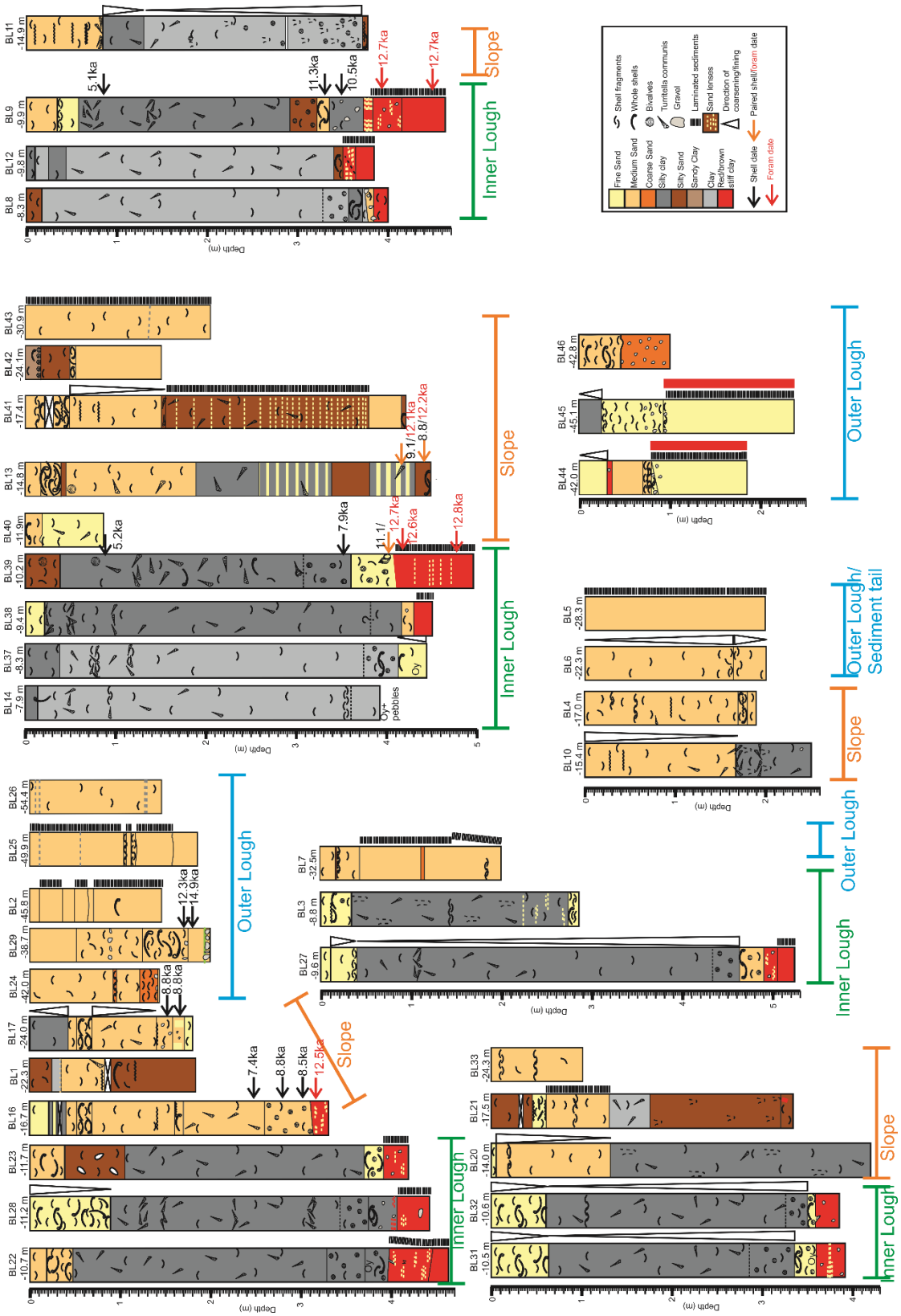

Supplementary Figure S2. Overview of the lithology of all acquired cores, with indication of dated samples. For the core locations, see Figure 1b.

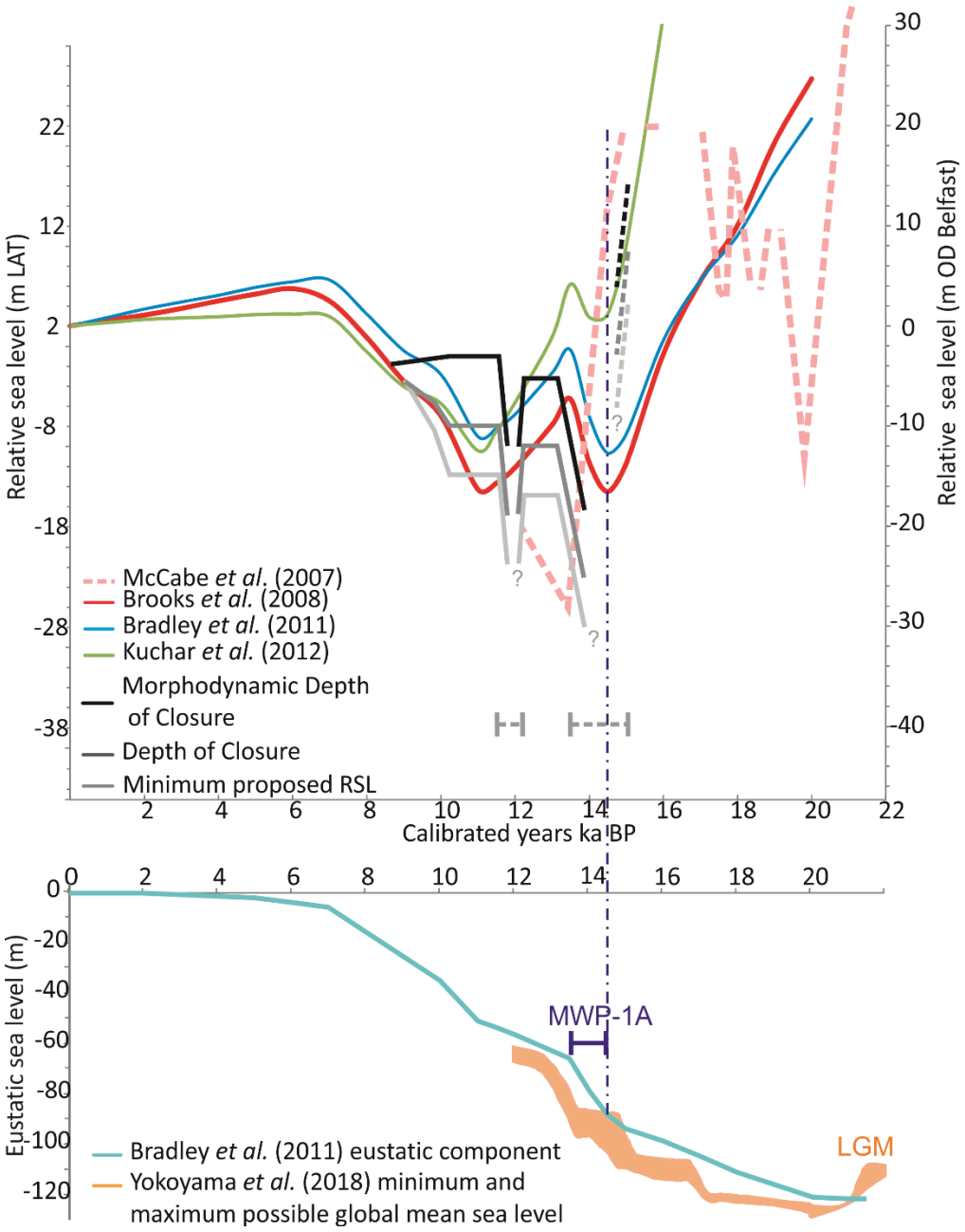

Supplementary Figure S3. Comparison between proposed, GIA derived and McCabe et al.'s (2007) reconstructions (see Figure 7c). The bottom graph shows Bradley et al.'s (2011) eustatic component versus Yokoyama et al.'s (2018) global mean sea level. The purple bar illustrates the interval between 14.5 and 13.5k cal a BP during which MWP-1A is introduced in the GIA model approach. Yokoyama et al.'s (2018) curve shows the possible stepped nature of MWP-1A with the potential timings of periods with rapid sea-level rise.